CHAPTER IV
RESULTS AND DISCUSSIONS

4.1 Characterization.

4.1.1 FT-IR Spectroscopy.

From FT-IR spectra of undoped and doped polyaniline, peaks were identified and summarized in Table 4.1. The peaks in the brackets were previously determined by other investigators.

Emeraldine base has essentially five FT-IR characteristic peaks as shown in Figure 4.1.1.1. Each peak position identifies a specific characteristic of emeraldine base which can be related to its chemical bonds.

The absorption peaks at 1584 and 1493 cm^{-1} represent the stretching vibration of the quinoid ring and the benzenoid ring, respectively (Zang *et al.* 1998). This indicates that the synthesized polyaniline is composed of two parts which are the feature of emeraldine base. The absorption peak at 1161 cm^{-1} indicates an electronic band which is associated with electrical conducting of polyaniline (Narayana *et al.* 1994). The last peak is at 824 cm^{-1} indicats the type of substituted benzene in polyaniline which is the para-disubstitution benzene ring (Milton and Monkman, 1993).

From Figures 4.1.1.2-4.1.1.4, FT-IR spectra of HBr, CSA, and maleic acid doped polyanilines show absorption peaks at 1496-1480, and 1297 cm^{-1} represent the stretching vibrations of N-benzenoid ring and aromatic C-N stretching vibration, respectively. Both of them can be found in undoped and doped polyanilines. The absorption peak at 1161 cm^{-1}, however, was found only in the undoped polyaniline, because the quinoid ring units were converted to benzenoid ring units. Moreover, all doped polyanilines elucidates the 1,2,4 substituent benzene rings which has the peak at about 878-866 cm^{-1}.

In case of maleic acid doped polyaniline, the absorption peak at 3056 cm^{-1} at a doping ratio (N_A/N_{EB} = 4) can be assigned to the carboxylic group of maleic acid. The appearance of the bands at 577, 1396, and 1636 cm^{-1} in FT-IR spectra at a higher doping ratio (N_A/N_{EB} = 1295) could be related to the vibrational modes of cyclic structures containing tertiary nitrogen formed by crosslinking (Pereira de Silva *et al.* 2000).

For maleic acid and CSA doped polyanilines, spectra show not only a new peak at around 1700 cm^{-1} representing the carbonyl group of remaining dopants, but also an absorption peak at around 1223 cm^{-1} reflecting the C-N stretching through a C-N-C angle due to the increase in planarity through changes in the conformation after doping (Levon *et al.* 1995). The sulfonic acid salt group generated from the sulfonic acids, in case of CSA doped polyaniline, is the cause of the absorption peak at 1035 cm^{-1} in FT-IR spectrum.

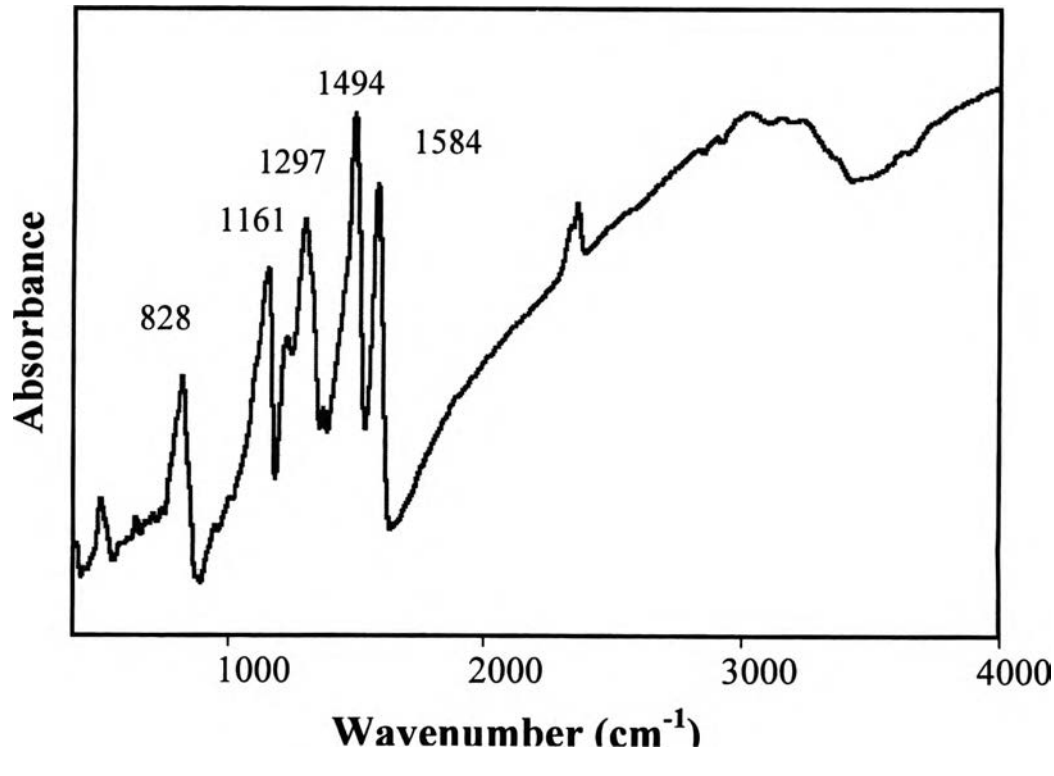

Figure 4.1.1.1 FT-IR spectra of polyaniline emeraldine base powder.

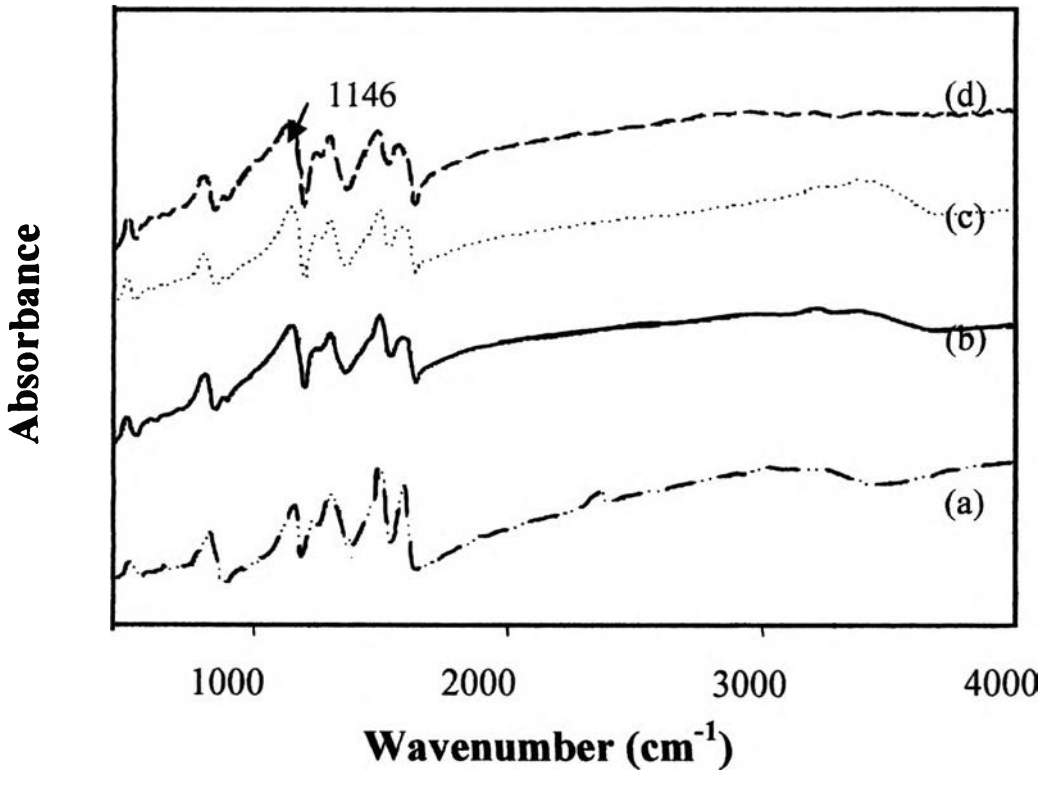

Figure 4.1.1.2 FT-IR spectrum of HBr doped polyaniline of at: (a) emeraldine base; (b) $N_A/N_{EB} = 4$; (c) $N_A/N_{EB} = 40$; and (d) $N_A/N_{EB} = 200$.

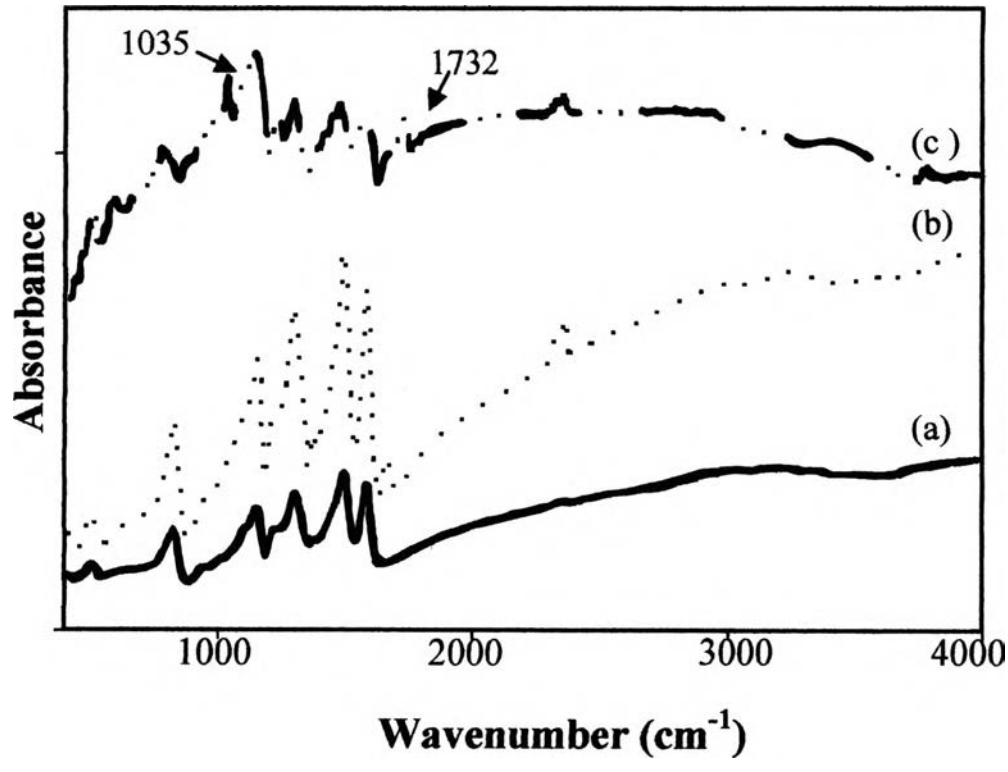

Figure 4.1.1.3 FT-IR spectrum of CSA doped polyaniline of at: (a) emeraldine base; (b) $N_A/N_{EB} = 4$; and (c) $N_A/N_{EB} = 200$.

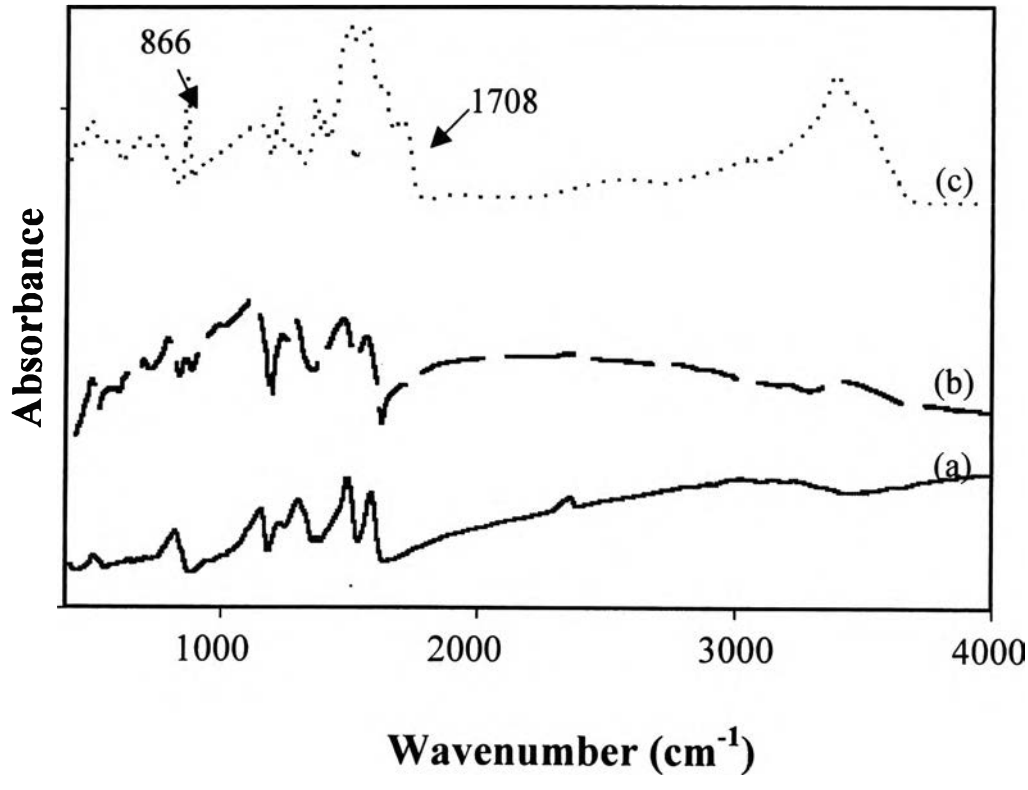

Figure 4.1.1.4 FT-IR spectrum of maleic acid doped polyaniline of at: (a) emeraldine base; (b) $N_A/N_{EB} = 4$; and (c) $N_A/N_{EB} = 200$.

Table 4.1 Assignments for FT-IR absorption bands of undoped and doped polyanilines.

Wavenumber (cm^{-1})						Assignments	References
PANI	PANI-HCl/HBr	PANI-HCl/MA	PANI-H_2SO_4/HNO_3*	PANI-H_2SO_4/HCOOH*	PANI-/CSA		
3242± 3	3377± 5	3393± 1	3247± 3 [3100-3500]	3230± 3	3234± 2	NH stretching	Kang *et al.*(1998)
		1705± 3			1732± 3 [1741]	Stretching of C=O group of acid	The Aldrich library of FT-IR Spectra
			1623± 2 [1600-1650]			Vibrational mode of covalent nitrate	Wade *et al.*, (1995)
1584± 2	1580± 6	1556± 3	1576± 1	1579± 5 [1595]	1557± 6	C=N stretching of quinoid ring	Milton and Monkman *et al.*, (1993)

Wavenumber (cm^{-1})						Assignments	References
PANI	PANI-HCl/HBr	PANI-HCl/MA	PANI-H_2SO_4/HNO_3*	PANI-H_2SO_4/HCOOH*	PANI-/CSA		
1493± 2	1496± 5	1496± 5	1537± 2	1496± 2 [1498]	1480± 1	Stretching of benzenoid ring	Zeng and Ko ,(1998)
			1344 ± 2 [1360-1430]			Vibrational mode of NO_3^-	Wade *et al.*, (1995)
1297± 4	1292± 3	1303± 4	1317± 1	1296± 2 [1306]	1300± 2	C-N stretching of benzenoid ring	Show-An Chen *et al.*, (1995)
		1223± 1	1228± 3 [1230]			C-N stretching through C-N-C angle	Levon *et al.*, (1995)
1155± 5			1175 ± 4 [1165]			Broken symmetry mode of quinoid structure	Chan *et al.*, (1994)

Wavenumber (cm^{-1})						Assignments	References
PANI	PANI-HCl/HBr	PANI-HCl/MA	PANI-H_2SO_4/HNO_3*	PANI-H_2SO_4/HCOOH*	PANI-/CSA		
	1146± 2 [1140]			1129± 3	1145± 7	A mode of $Q=N^+H$-B or B-NH-B	Morales *et al.*, (1977)
					1035± 6 [1059]	Sulfonic acid salt group	The Aldrich library of FT-IR Spectra
			917± 1 [800-860]			Vibrational mode of NO_3^-	Wade *et al.*, (1995)
	878± 1 [850-910]	866± 2				C-H out of plane bending of 1,2,4 ring	Zeng and Ko (1998)
824± 3			836± 1 [825]	817± 1		Out of plane bending of 1,4-ring	Milton and Monkman (1993)

Wavenumber (cm^{-1})						Assignments	References
PANI	PANI-HCl/HBr	PANI-HCl/MA	PANI-H_2SO_4/HNO_3*	PANI-H_2SO_4/HCOOH*	PANI-/CSA		
			764 ± 4 [740]		779± 5	C-H out of plane bending of 1,2-ring	Kang *et al.*(1998)

N_A/N_{EB} = 4, 40, 200, 400

* Data taken from Amornlertratanatada (2001).

[ ] Data taken from the references.

4.1.2 UV-Visible Spectroscopy.

The optical properties have played a key role in the elucidation of the basic electronic structure in the conducting polymers. Significant changes in their optical absorption are always accompanied with changes in chemical structure, quality of the solvents, temperature, and extent of doping (Zheng *et al.* 1994). Figure 4.1.2.1 shows UV-Visible spectra of synthesized emeraldine base in NMP solvent. The important peaks occurred which can be illustrated in the Table 4.2 below.

Emeraldine base has two classic absorptions. The first one is at 324 nm which is attributed to the π-π^* transition associated with π electrons of the benzene ring delocalized on nitrogen atoms of the amine group (Sertova *et al.* 1998). The second one at 633 nm is assigned to the excitation from the highest occupied molecular orbital (HOMO, π_b) of the three-ring benzenoid part of the system to the lowest unoccupied molecular orbital (LUMO, π_q) of the localized quinoid ring with the two surrounding imine nitrogen (Zheng *et al.* 1994).

For both of CSA and maleic acid doped polyaniline, Figure 4.1.2.3 and 4.1.2.4, they could still be seen that the two absorption peaks exhibiting in emeraldine base can still be observed at the lowest doping ratio (N_A/N_{EB} = 4) because the concentrations of CSA and maleic acid dopants at this doping ratio were not enough to convert emeraldine base to emeraldine salt. At higher doping ratio (N_A/N_{EB} = 4), the absorption peak at 633 nm for both acid doped polyanilines completely disappeared. Therefore, a stronger acid doped needed a lesser amount of acid dopant for converting an undoped polyaniline to a doped emeraldine. The absorption peak at around 700-900 nm, furthermore, was observed due to lacalized polaron band. The shoulder absorption at about 440 nm was assigned changing of the quinoid segments to the bipolaron state (Olinga *et al.* 2000). Recently, it is suggested that the polaron or semiquinone form is primarily resident in the ordered crystalline regions of the emeraldine

salt, whereas the bipolaron form is primarily in the amorphous regions. At higher doping ratio (N_A/N_{EB} = 40), the absorption peak at 633 nm of CSA doped polyaniline completely disappeared. Therefore, a stronger acid doped needs a lesser amount of acid dopant for converting an undoped polyaniline to a doped one.

For a weak acid, maleic acid, doped polyaniline, the absorption peak was still presented at 325 and 618 nm at low doping ratio (N_A/N_{EB} = 4). It was indicated that the concentration of maleic acid was not enough to protonate emeraldine base. At higher doping ratio (N_A/N_{EB} = 40), it showed the absorption peaks at 314, 425, 627, and 819 nm. This indicated that emeraldine base was partially protonated with maleic acid because of the remaining of quinoid parts.

However, at higher doping ratio (N_A/N_{EB} = 80), it illustrated the absorption peaks at 325, 430, and 820 nm, presenting benzenoid parts, bipolaron state, and polaron state, respectively, that meant polyaniline was fully doped with maleic acid peaks. At higher doping ratio (N_A/N_{EB} = 80) maleic doped polyaniline showed the absorption peaks at around 320, 440, and 650 nm that meant no polaron state was observed while bipolaron state was seen. This indicated that polyaniline was absolutely fully protonated at the quinoid parts. hence the mobility of electrons along their chains and from chain to chain reduced. The localized polaron state, nevertheless, appeared again at the absorption peak about 700 nm at very high doping ratios (N_A/N_{EB}= 1295). This indicated that maleic acid doped polyaniline was a reversible process as shown in Scheme 4.1.

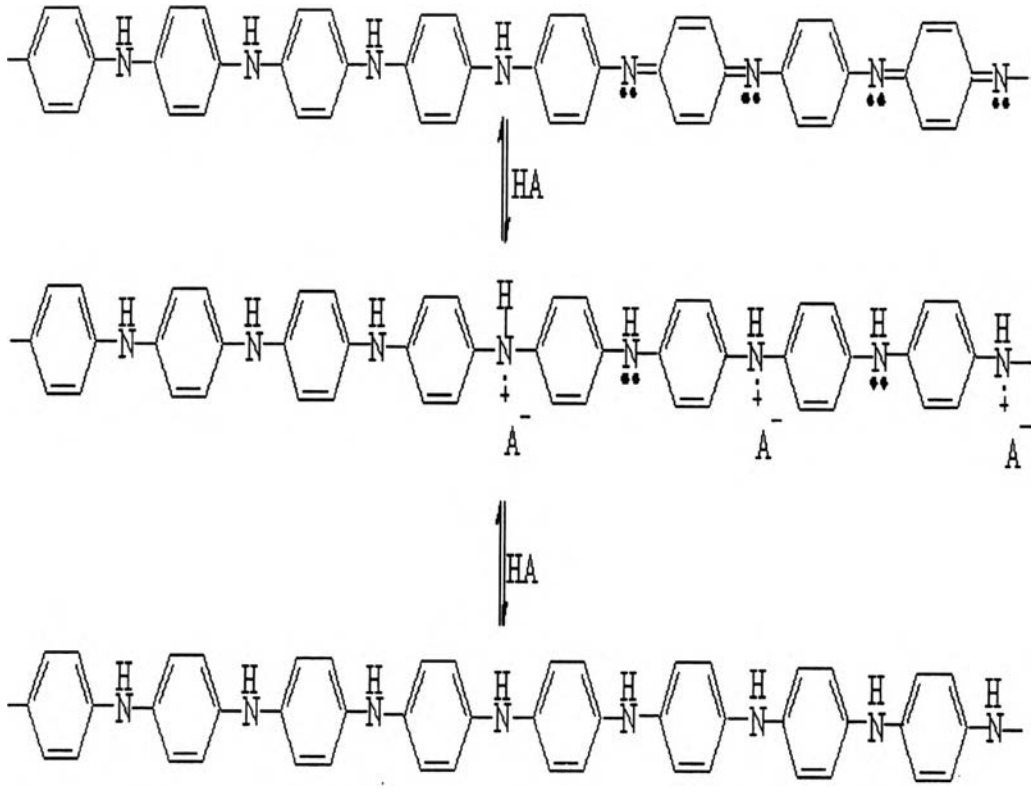

Scheme 4.1 The schematic of maleic acid doped polyaniline which is a reversible process.

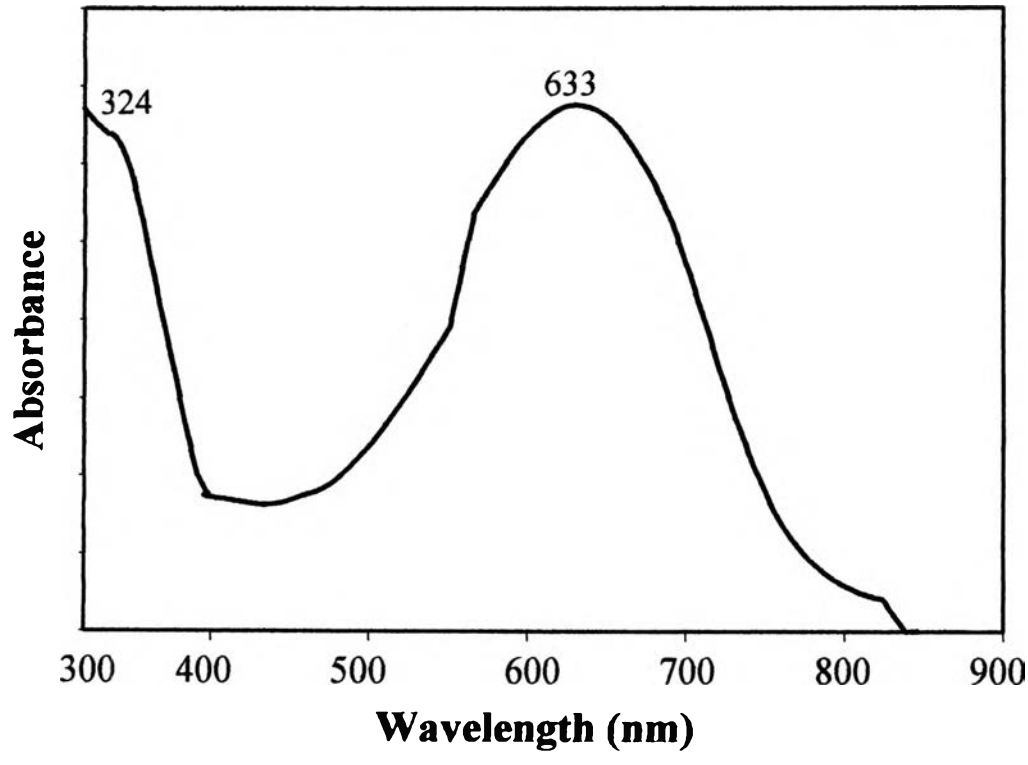

Figure 4.1.2.1 UV-Visible spectra of undoped polyaniline emeraldine base.

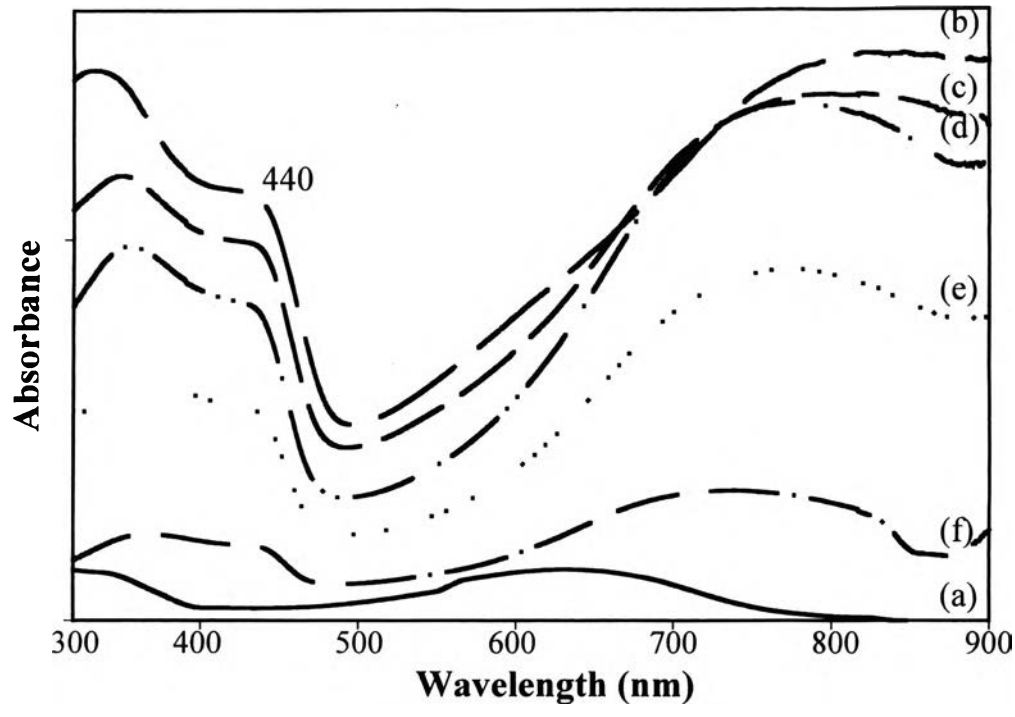

Figure 4.1.2.2 UV-Visible spectrum of HBr doped polyaniline of: (a) emeraldine base; (b) $N_A/N_{EB} = 4$; (c) $N_A/N_{EB} = 40$; (d) $N_A/N_{EB} = 200$; (e) $N_A/N_{EB} = 400$; and (f) $N_A/N_{EB} = 1295$.

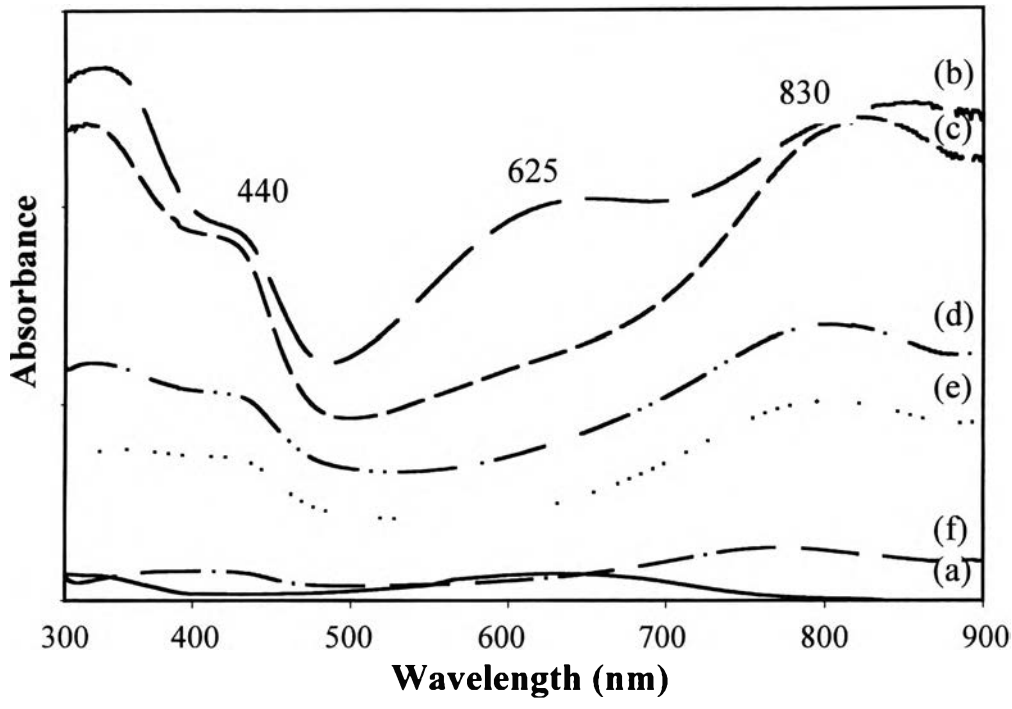

Figure 4.1.2.3 UV-Visible spectrum of CSA doped polyaniline of: (a) emeraldine base; b) N_A/N_{EB} = 4; (c) N_A/N_{EB} = 40; (d) N_A/N_{EB} = 200; (e) N_A/N_{EB} =400; and (f) N_A/N_{EB} = 1295.

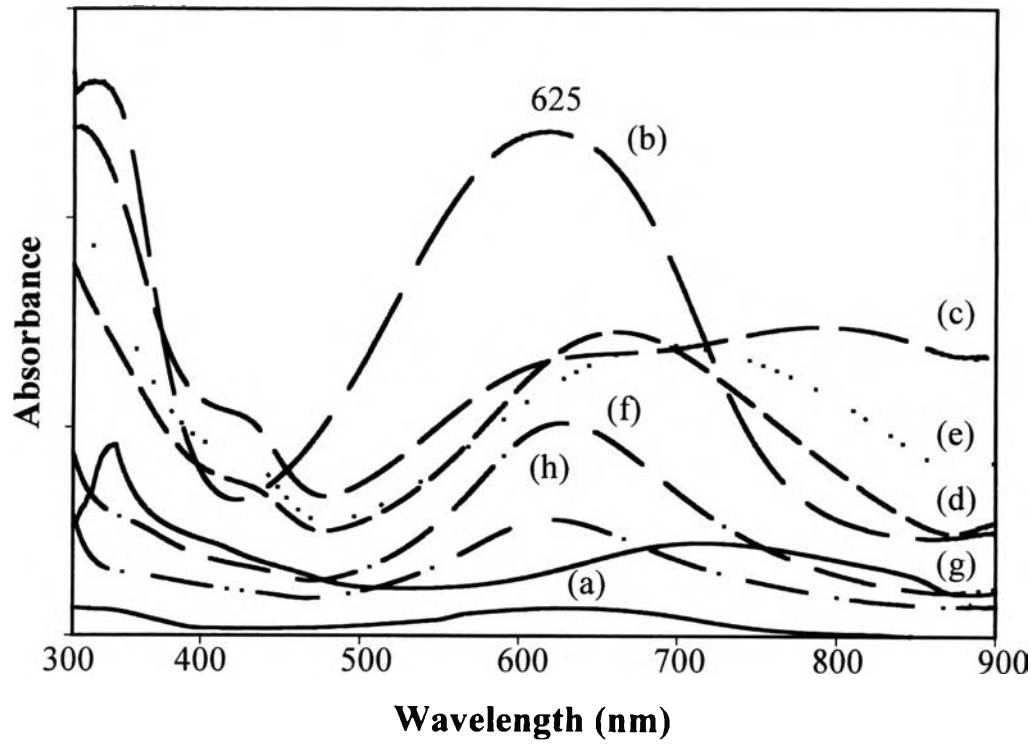

Figure 4.1.2.4 UV-Visible spectrum of maleic acid doped polyaniline of: (a) emeraldine base; (b) N_A/N_{EB} = 4; (c) N_A/N_{EB} = 20; (d) N_A/N_{EB} = 50; (e) N_A/N_{EB} = 200; (f) N_A/N_{EB} = 400; (g) N_A/N_{EB} = 1295.

Table 4.2 Assignments for UV-Visible spectrum of undoped and doped polyanilines at fully doped state.

Wavelength (nm)						Assignments	References
PANI	PANI-HCl/HBr	PANI-HCl/MA	PANI-H_2SO_4/HNO_3*	PANI-H_2SO_4/HCOOH*	PANI-/CSA		
324 [325]	332	314	317	317	325	Transition of the EB benzene ring	Sertova *et al.*, 1998
	434	430	435	432	430 [425]	Changing of quinoid segments to the bipolaron state	Hunag *et al.*, 1993
633 [630]		650			635-697	The excitation of quinoid ring	Wan *et al.*, 1992
			763 [764]			The positive radical of the polaron state in the polyaniline salt	Pereira du silva *et al.*, 1993
	841	792		780 [780]		Localized polaron	Zheng *et al.*, 1992

* Data taken from Amornlertratanatada (2001).

[ ] Data taken from the references.

Table 4.3 Assignments for UV-Visible spectrum of doped polyanilines at various doping ratios.

Wavelength (nm)						Assignments	References
N_A/N_{EB}	PANI-HCl/HBr	PANI-HCl/MA	PANI-H_2SO_4/HNO_3*	PANI-H_2SO_4/HCOOH*	PANI-/CSA		
4	332 [325]	317	314	317	325	Transition of the EB benzene ring	Sertova *et al.*, 1998
	440 [425]			440		Changing of quinoid segments to the bipolaron state	Huang *et al.*, 1993
		616	597		635 [630]	The excitation of quinoid ring	Wan *et al.*, 1992
	821			787 [780]		Localized polaron	Zheng *et al.*, 1992
40	350	314	317	320	325 [325]	Transition of the EB benzene ring	Sertova *et al.*, 1998
	440	430		430 [425]		Changing of quinoid segments to the bipolaron state	Huang *et al.*, 1993

Wavelength (nm)						Assignments	References
N_A/N_{EB}	PANI-HCl/HBr	PANI-HCl/MA	PANI-H_2SO_4/HNO_3*	PANI-H_2SO_4/HCOOH*	PANI-/CSA		
40		650			635 [630]	The excitation of quinoid ring	Wan *et al.*, 1992
	819	792	763	769 [780]		Localized polaron	Zheng *et al.*, 1992
200	351	289	309	285	325 [325]	Transition of the EB benzene ring	Sertova *et al.*, 1998
	440	435	430	435	435 [425]	Changing of quinoid segments to the bipolaron state	Huang *et al.*, 1993
		655 [630]			697	The excitation of quinoid ring	Wan *et al.*, 1992
	770 [780]		773	790		Localized polaron	Zheng *et al.*, 1992
400	358	287	306	286	328 [325]	Transition of the EB benzene ring	Sertova *et al.*, 1998

Wavelength (nm)						Assignments	References
N_A/N_{EB}	PANI-HCl/HBr	PANI-HCl/MA	PANI-H_2SO_4/HNO_3*	PANI-H_2SO_4/HCOOH*	PANI-/CSA		
400	440	440	435 [425]	432	432	Changing of quinoid segments to the bipolaron state	Huang *et al.*, 1993
		627 [630]			648	The excitation of quinoid ring	Wan *et al.*, 1992
	744		794 [780]	717		Localized polaron	Zheng *et al.*, 1992

* Data taken from Amornlertratanatada (2001).

[ ] Data taken from the references.

4.1.3 Thermogravimetric Analyzer (TGA).

Thermogravimetric analysis under nitrogen atmosphere of emeraldine base indicates three major step weight losses as shown in Figure 4.1.3.1. The first one was between 40°C due to solvent molecules. The loss of residual water molecules and other solvents was evident at about 100°C. The other loss was at about 500°C indicating the degradation of polymer chains (Palaniappan and Narayana. (1994). For all protonic acid doped polyanilines, four important step weight loss behaviors occurred as shown in Figure 4.1.3.2-4.1.3.4. Water molecules evaporated from polymer chains accounting for 4-5% by weight occurred at about 75, 128 and 119°C for HBr doped polyanilines, maleic acid doped polyanilines, and CSA doped polyanilines, respectively. Due to the loss of the dopants, the thermograms show the third step weight loss at about 218, 198, and 200°C for HBr doped polyanilines, maleic acid doped polyanilines, and CSA doped polyanilines, respectively. The last step representing the structural decomposition of the polymer backbone was evident at about 500°C. The weight loss temperatures of the doped and undoped polyanilines are summarized in Table 4.3 below.

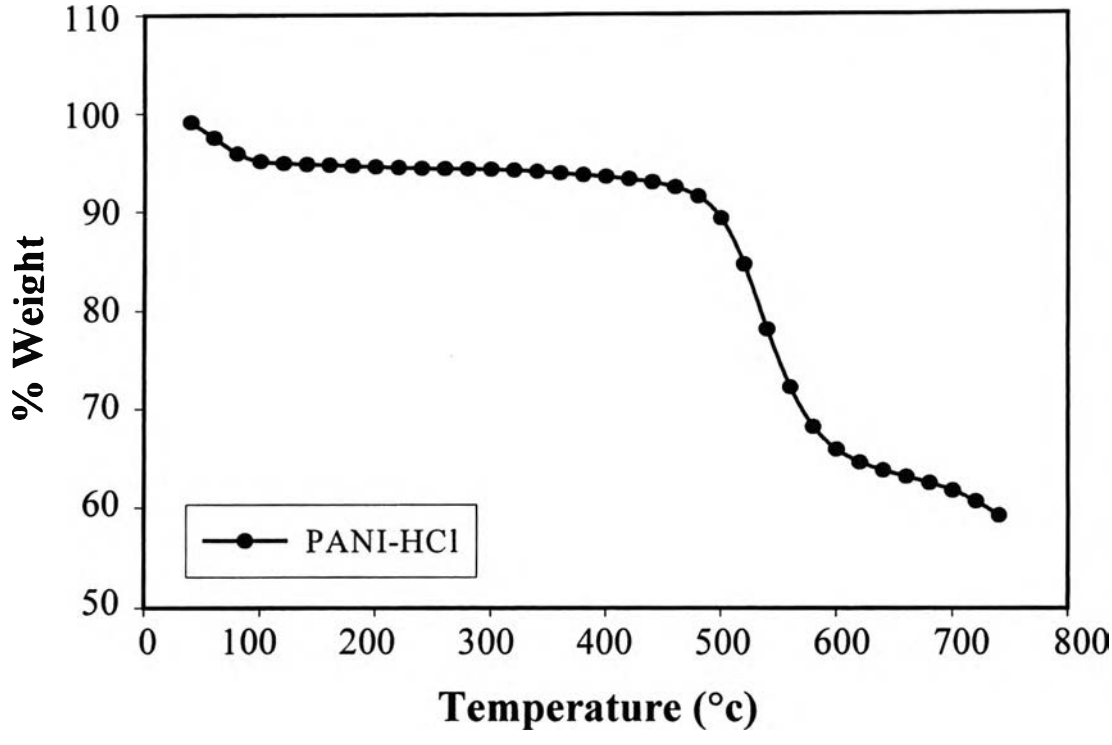

Figure 4.1.3.1 The TGA thermogram of polyaniline emeraldine base powder.

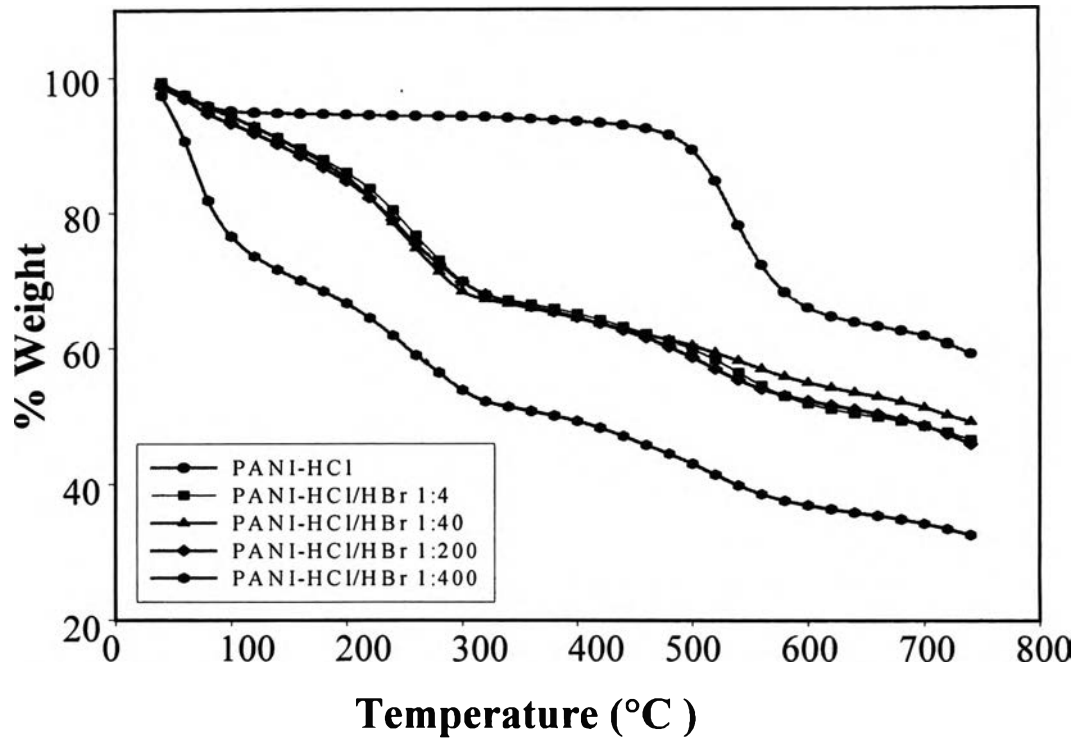

Figure 4.1.3.2 The TGA thermograms of polyaniline emeraldine base and HBr doped polyaniline at various doping ratios.

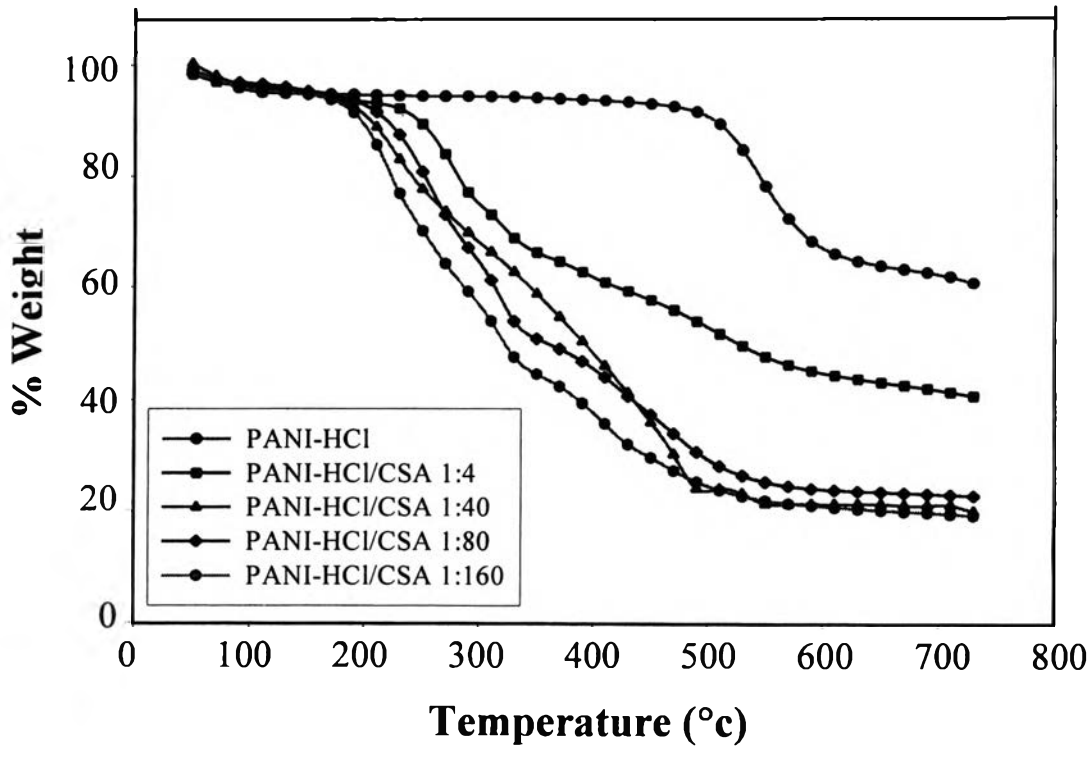

Figure 4.1.3.3 The TGA thermograms of polyaniline emeraldine base and CSA doped polyaniline at various doping ratios.

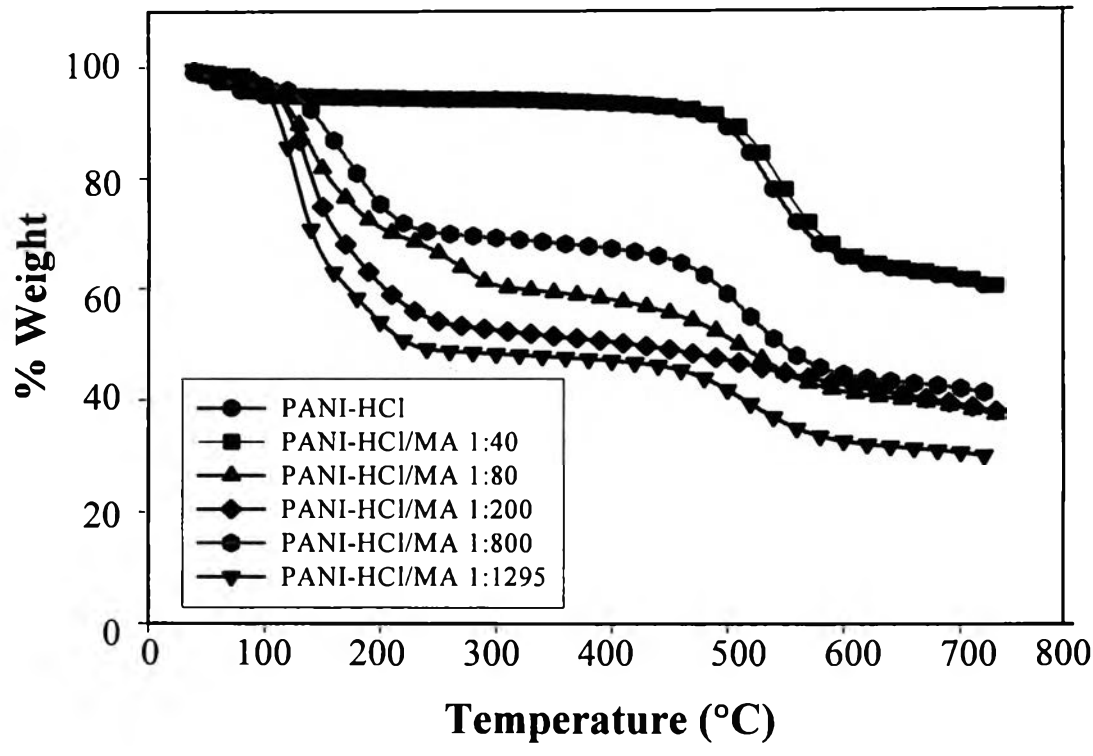

Figure 4.1.3.4 The TGA thermograms of polyaniline emeraldine base and maleic acid doped polyaniline at various doping ratios.

Table 4.4 Assignments for TGA thermograms of undoped and doped polyanilines.

Temperature (°C)						Assignments	References
PANI	PANI-HCl/HBr	PANI-HCl/MA	*PANI-H_2SO_4/NA	*PANI-H_2SO_4/FA	PANI/CSA		
39±5 [42]	48±8	44±6	55±8	49±14	53±10	The loss of solvent molecules (THF and Methanol)	Li *et al.*, 1999
106±6 [110]	75±6	128±7	97±11	106±7	119±28	The loss of water molecule	Palaniappan *et al.*, 1994
-	218±31	198±20	116±9 [110-275]	245±15	288±18	The loss of acid molecule as volatile gas	Palaniappan *et al.*, 1994
522±19 [500]	557±28	521±4	505±25	504±16	478±12	Degradation of polymer backbone	Li *et al.*, 1999

- Data taken from Amornlertratanatada (2001).

[ ] Data taken from the references.

4.1.4 X-ray diffration.

XRD techinique was used to investigate the order and the degree of crystallinity of polyanilines. The XRD data were analyzed in term of the Bragg's law: $2d\sin\theta = n\lambda$, while the d-value represents the distance between lattices planes. The theta positions determine a unit cell orientation.

In Figure 4.1.4.1, it shows that the diffraction patterns of emeraldine base was typically of an amorphous polymer. On the other hand, all protonic acid doped polyanilines were semicrystalline polymers, as shown in Figures 4.1.4.2-4.1.4.4. They can be distinguished: the crystalline one corresponds to a relative sharp peak, Bragg-type reflection peaks; and the amorphous one is visible as a broad and low-intensity halo (Lunzy et Banka, 2000). Table 4.5 shows the value of 2theta and d-value of undoped and doped polyanilines investigated.

For emeraldine base, the amorphous polymer possibly has a compact coil structure resulting from the H-bonding between amine and imine positions. When polyaniline was protonated by acid dopants, the protonation of N positions occurred inducing the positive charges along the chain. So an expansion of the polyaniline coils structure was observed resulting in crystalline structures. The partially crystallinity was also observed at low doping ratio, causing a larger distance between polymer chain and a corresponding high d- value, because of the lesser repulsion forces between the positive charges along the chain. At higher doping ratios, in contrast, the expanded chains were present as evidenced by the lower d-value as the polymer chains could pack together closer.

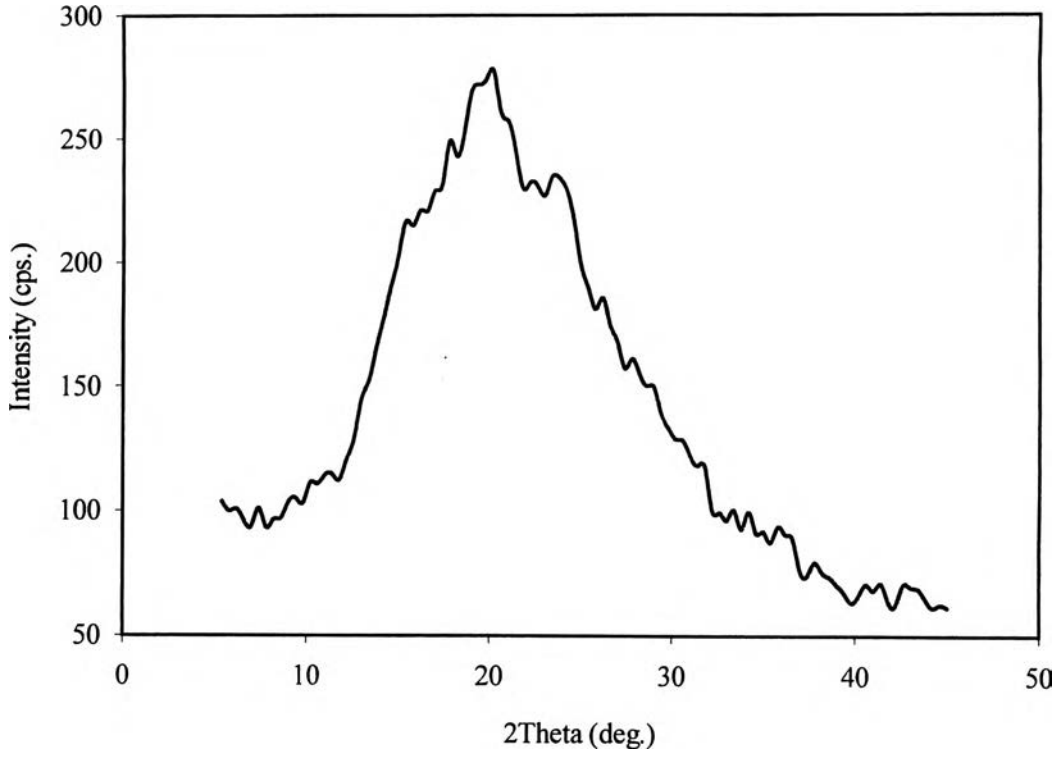

Figure 4.1.4.1 XRD diffration pattern of polyanilne emeraldine base.

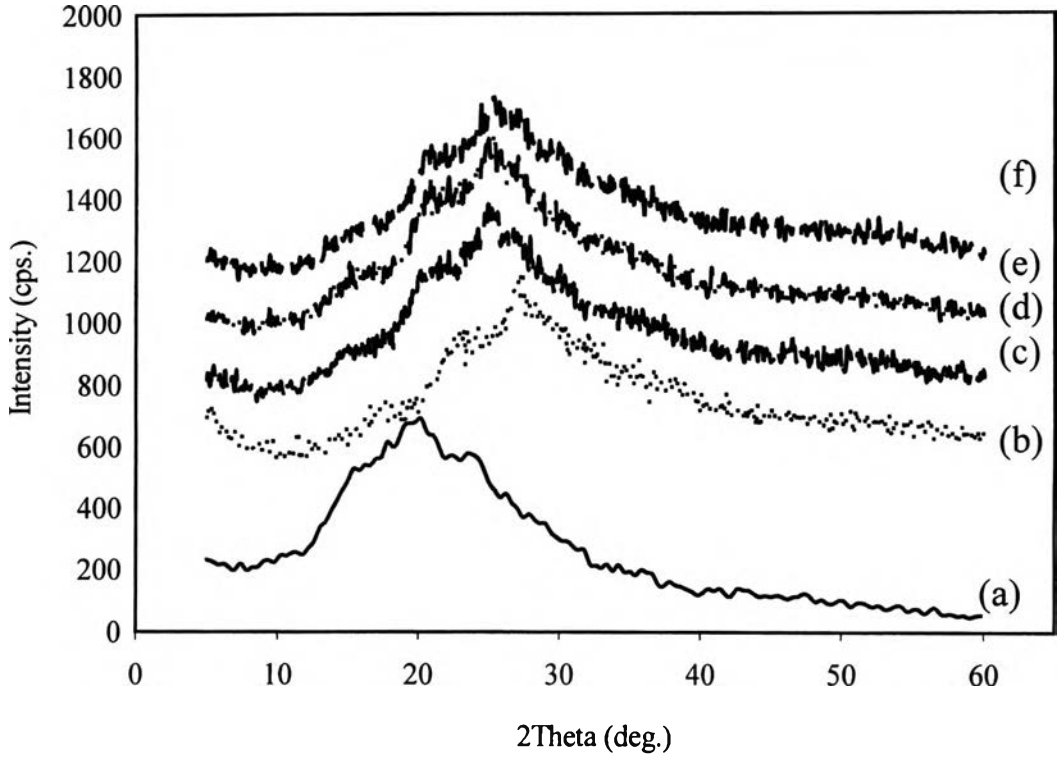

Figure 4.1.4.2 XRD diffraction patterns of polyaniline emeraldine base and HBr doped polyaniline at various doping ratios: (a) N_A/N_{EB}=0; (b) N_A/N_{EB}=4; (c) N_A/N_{EB}=40; (d) N_A/N_{EB}=200; (e) N_A/N_{EB}=400; and (f) N_A/N_{EB}=1295.

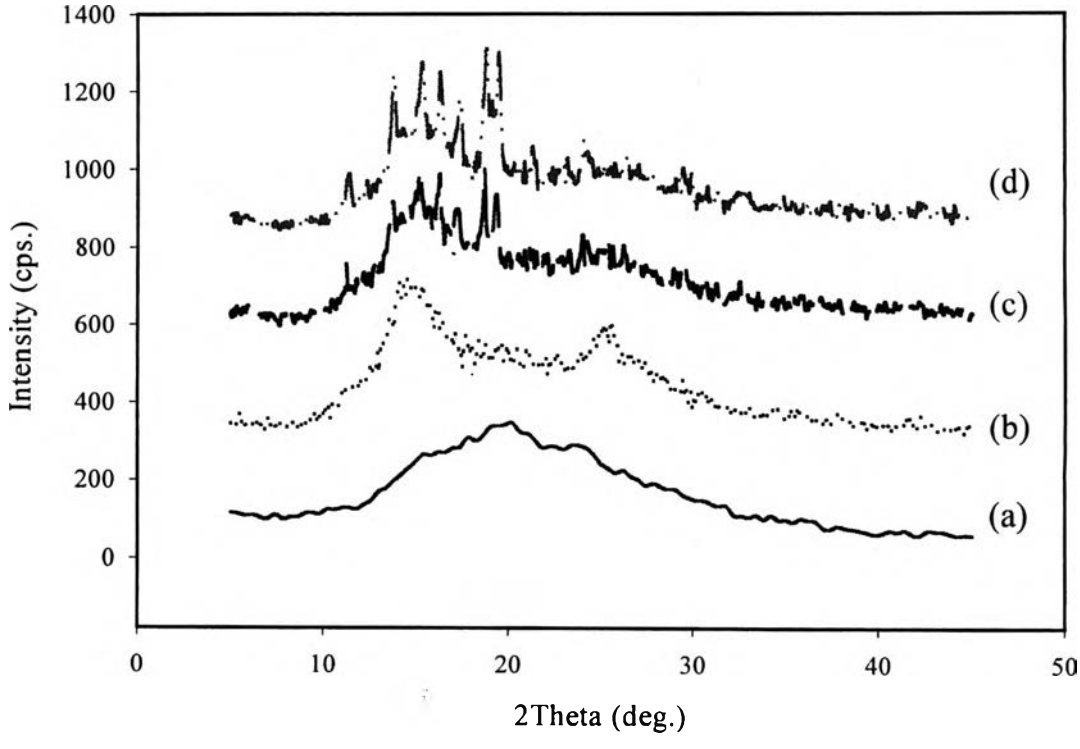

Figure 4.1.4.3 XRD diffraction patterns of polyaniline emeraldine base and CSA doped polyaniline at various doping ratios: (a) $N_A/N_{EB}=0$; (b) $N_A/N_{EB}=20$; (c) $N_A/N_{EB}=80$; and (d) $N_A/N_{EB}=200$.

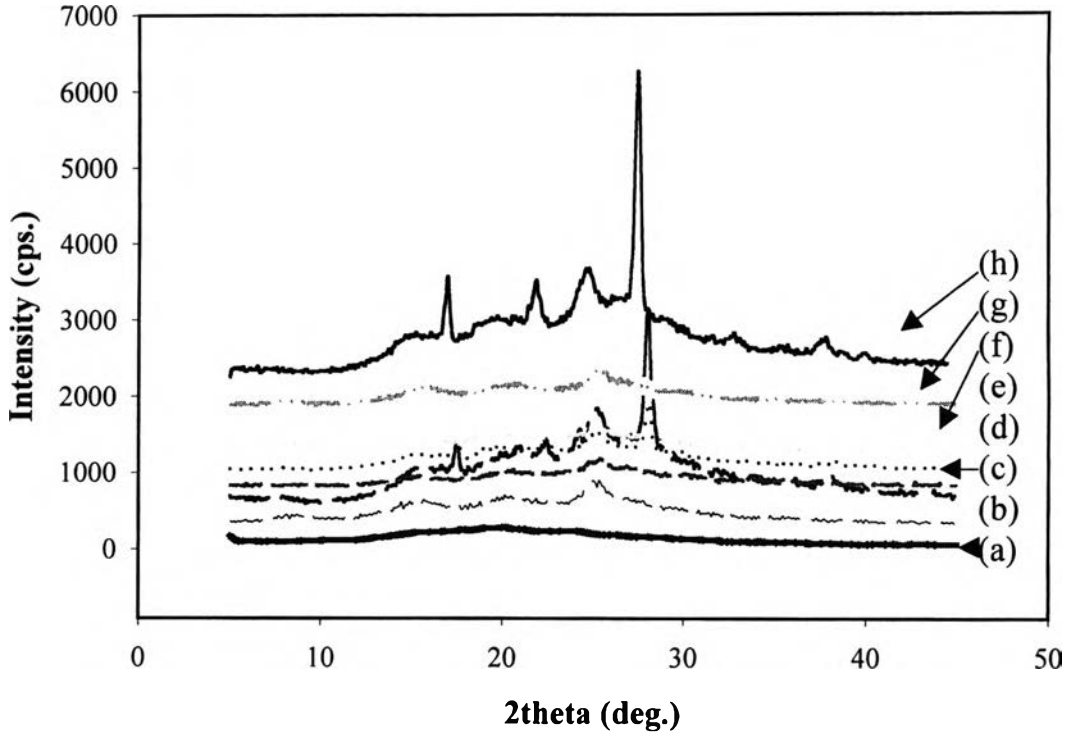

Figure 4.1.4.4 XRD diffraction patterns of polyaniline emeraldine base and maleic acid doped polyaniline at various doping ratios: (a) N_A/N_{EB}=0; (b) N_A/N_{EB}=20; (c) N_A/N_{EB}=40; (d) N_A/N_{EB}=200; (e) N_A/N_{EB}=400; (f) N_A/N_{EB}=500; (g) N_A/N_{EB}=800; and (h) N_A/N_{EB}=1295.

Table 4.5 The value of 2theta and d-value of undoped and doped polyanilines.

Sample	N_A/N_{EB}	2Theta (deg.)	d-value (A°)
PANI-HCl	-	19.40, 19.53	4.57, 4.59
		36.60, 36.63	2.45, 2.50
PANI-HCl/HBr	1293	9.44, 9.45	9.36, 9.40
		15.10, 15.21	5.86, 5.89
		20.52, 20.54	4.32, 4.35
		24.98, 25.02	3.56, 3.59
		26.92, 26.96	3.31, 3.39
		29.78, 29.82	2.99, 3.04
	400	20.44, 20.48	4.34, 4.39
		25.02, 25.03	3.56, 3.58
		27.08, 27.12	3.29, 3.33
	200	15.32, 15.22	5.78, 5.82
		20.65, 21.00	4.31, 4.23
		25.10, 25.16	3.54, 3.54
		27.10, 27.36	3.29, 3.26
	160	15.38, 15.88	5.76, 5.58
		21.04, 21.20	4.22, 4.19
		25.00, 25.02	3.56, 3.56
		27.14, 26.88	3.28, 3.31
	80	15.20, 15.22	5.82, 5.84
		20.68, 20.71	4.29, 4.29
		25.02, 25.04	3.56, 3.57
	4	9.40, 9.43	9.40, 9.42
		14.88, 14.91	5.95, 5.96
		20.68, 20.73	4.29, 4.31

Sample	N_A/N_{EB}	2Theta (deg.)	d-value (A°)
		25.22, 25.26	3.53, 3.55
		30.62, 30.65	2.92, 2.96
PANI-HCl/CSA	160	11.48, 11.36	7.70, 7.78
		13.94, 13.82	6.35, 6.40
		14.40, 14.36	6.15, 6.16
		15.48, 15.32	5.72, 5.78
		16.48, 16.32	5.37, 5.42
		17.52, 17.40	5.05, 5.09
		18.90, 18.78	4.69, 472
		19.58, 19.44	4.53, 4.56
		21.42, 21.32	4.14, 4.16
		24.24, 24.02	3.67, 3.70
	40	15.50, 15.24, 15.00	5.71, 5.81, 5.70
		16.52, 16.24, 16.62	5.36, 5.45, 5.33
		17.52, 17.30, 17.28	5.06, 5.12, 5.13
		18.94, 18.68, 18.26	4.68, 4.45, 4.85
		21.50, 21.22, 21.12	4.13, 4.18, 4.22
		24.30, 24.80, 24.28	3.66, 3.89, 3.66
	20	15.04, 15.05	5.89, 5.93
		25.18, 25.20	3.53, 3.54
	4	14.66, 14.84	6.04, 5.96
		25.20, 25.06	3.53, 3.55
	2	14.80, 14.83	5.98, 6.01
		25.20, 25.22	3.53, 3.54
PANI-HCl/MA	1293	17.48, 17.52, 17.50	5.07, 5.06, 5.06
		22.38, 22.42, 22.42	3.97, 3.96, 3.96
		25.08, 25.10, 25.20	3.55, 3.54, 3.53

Sample	N_A/N_{EB}	2Theta (deg.)	d-value (A°)
		24.88, 24.89	3.58, 3.60
		26.98, 26.70	3.30, 3.33
	200	11.38, 11.41	7.77, 7.78
		14.36, 14.37	6.16, 6.18
		19.48, 19.50	4.64, 4.67
		21.38, 21.39	4.15, 4.18
		24.02,24.03	3.70, 3.72
		25.34, 25.36	3.51, 3.53
	40	11.32, 11.35	7.81, 7.83
		13.76, 13.79	6.43, 6.46
		15.28, 15.31	5.79, 5.82
		16.28, 16.32	5.44, 5.46
		17.28, 17.32	5.13, 5.16
		18.68, 18.71	4.75, 4.78
		19.36, 19.37	4.58, 4.59
	30	15.12, 15.15	5.85, 5.85
		250.4, 25.08	3.55, 3.57
	10	15.12, 15.16	5.85, 5.86
		25.18, 25.22	3.53, 3.53
	4	15.06, 14.66	5.88, 6.04
		25.30, 25.20	3.52, 3.53
PANI-H_2SO_4/CSA*	1293	15.72, 15.75	5.82, 5.84
		20.18, 20.23	4.39, 4.40
		25.08, 25.10	3.55, 3.58
		27.10, 27.11	3.29, 3.33
		29.38, 29.42	3.04, 3.04
	400	15.28, 15.28	5.79, 5.80

Sample	N_A/N_{EB}	2Theta (deg.)	d-value (A°)
		20.16, 20.18	4.40, 4.42
		24.62, 24.68	3.61, 3.63
		26.34, 26.36	3.38, 3.39
		26.46, 26.48	3.37, 3.38
	200	15.02, 15.05	5.89, 5.92
		20.58, 20.59	4.31, 4.35
		25.08, 25.10	3.55, 3.57
		26.92, 26.95	3.31, 3.32
		29.72, 29.73	3.00, 3.02
	160	11.50, 11.38	7.69, 7.77
		15.46, 15.36	5.73, 5.76
		18.90, 18.78	4.69, 4.72
		19.60, 19.48	4.53, 4.55
	40	14.92, 15.26, 15.28	5.93, 5.80, 5.79
		19.40, 20.18, 19.36	4.57, 4.39, 4.58
PANI-H_2SO_4/FA*	400	9.46, 9.51	9.34, 9.35
		15.28, 15.29	5.79, 5.79
		20.16, 20.19	4.40, 4.42
		24.62, 24.64	3.61, 3.61
	200	15.44, 15.02	5.73, 5.89
		24.50, 25.08	3.63, 3.55
	50	15.78, 15.79	5.61, 5.62
		24.30, 24.34	3.66, 3.68
	4	15.00, 15.03	5.90, 5.92
		20.20, 20.22	4.39, 4.40
		24.96, 24.98	3.56, 3.58
		29.30, 29.33	3.05, 3.06

* Data taken from Amornlertratanatada (2001).

Sample	N_A/N_{EB}	2Theta (deg.)	d-value (A°)
		20.16, 20.18	4.40, 4.42
		24.62, 24.68	3.61, 3.63
		26.34, 26.36	3.38, 3.39
		26.46, 26.48	3.37, 3.38
	200	15.02, 15.05	5.89, 5.92
		20.58, 20.59	4.31, 4.35
		25.08, 25.10	3.55, 3.57
		26.92, 26.95	3.31, 3.32
		29.72, 29.73	3.00, 3.02
	160	11.50, 11.38	7.69, 7.77
		15.46, 15.36	5.73, 5.76
		18.90, 18.78	4.69, 4.72
		19.60, 19.48	4.53, 4.55
	40	14.92, 15.26, 15.28	5.93, 5.80, 5.79
		19.40, 20.18, 19.36	4.57, 4.39, 4.58
PANI-H_2SO_4/FA*	400	9.46, 9.51	9.34, 9.35
		15.28, 15.29	5.79, 5.79
		20.16, 20.19	4.40, 4.42
		24.62, 24.64	3.61, 3.61
	200	15.44, 15.02	5.73, 5.89
		24.50, 25.08	3.63, 3.55
	50	15.78, 15.79	5.61, 5.62
		24.30, 24.34	3.66, 3.68
	4	15.00, 15.03	5.90, 5.92
		20.20, 20.22	4.39, 4.40
		24.96, 24.98	3.56, 3.58
		29.30, 29.33	3.05, 3.06

* Data taken from Amornlertratanatada (2001).

Table 4.6 Comparison of experimental 2theta obtained from undoped and doped polyanilines with the results of model calculations.

2theta (deg.)	d-value (A°)	Reflection	References
9.44	9.3610	(010)	Winokur *et al.*, (1998)
15.10	5.8625	(100)	
20.52	4.3246	(040)	
24.98	3.5617	(110)	
26.92	3.3092	(012)	
29.78	2.9976	(112)	

4.1.5 Scanning Electron Microscope (SEM).

The undoped and doped polyaniline powder was studied in order to identify and to understand the relations between microstructures and electrical properties. According to Figures 4.1.5.1 and 4.1.5.2, the morphology of undoped polyaniline is similar to that of HBr doped polyaniline which was globular structure. Chen *et al.* (1991) reported that the granular morphology was seen in the undoped polyaniline which was synthesized by chemical method. On the other hand, by the electrochemical synthesized undoped polyaniline had a fibrillar network morphology. When polyaniline powder was protonated with any concentration of acid without applied any force, the loose loop structures were observed resulting from the partially protonation at nitrogen atoms causing some repulsion between the positive charges and the forming of intra-molecular hydrogen bonding between amine and imine positions. For doping ratio 4 of CSA doped polyaniline, the globular structure as shown in Figure 4.1.5.3 can be observed because the repulsion forces between positive charge along the chain were not sufficient to separate the chains. However, the fibrillar structure can be seen at doping ratios of 40, 80,

and 160 due to not only the repulsive forces between positive charge along the chain but also the intermolecular hydrogen bonding. It is interesting to observe that upon increasing the doping ratio, the morphology of the conductive polymer changed from having typical three dimensional random coil, granular structure to rigid rod-like, fibrillar structures. The globular structures of MA doped polyaniline can be observed at doping ratios of 4 and 40 according to Figure 4.1.5.4. For doping ratio 200 of maleic acid doped polyaniline, the fibrillar structure appeared due to a greater degree of intermolecular hydrogen bonding. Nevertheless, the globular structure of maleic acid doped polyaniline was surprisingly present at doping ratio of 500. It occurred because doping process of maleic acid doped polyaniline was a reversible process. The compact coil structure of the polyaniline originated from the intra-molecular hydrogen bonding. It was confirmed by the result of UV-Visible spectroscopy in the Figures 4.1.2.4 and 4.1.2.5. The structure of maleic doped polyaniline related to SEM micrographs is proposed and shown in Figure 4.1.5.5. These morphological structures are consistent with the results of XRD diffraction patterns as seen in Figures 4.1.4.1-4.1.4.4.

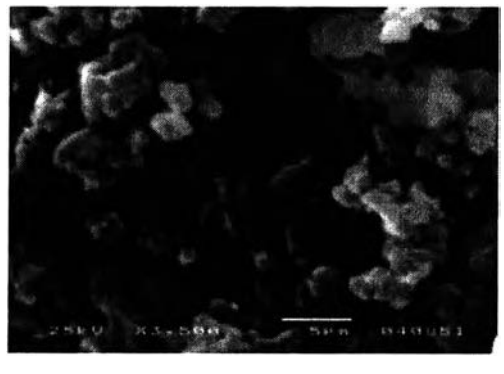

Figure 4.1.5.1 The morphological structure of undoped polyaniline.

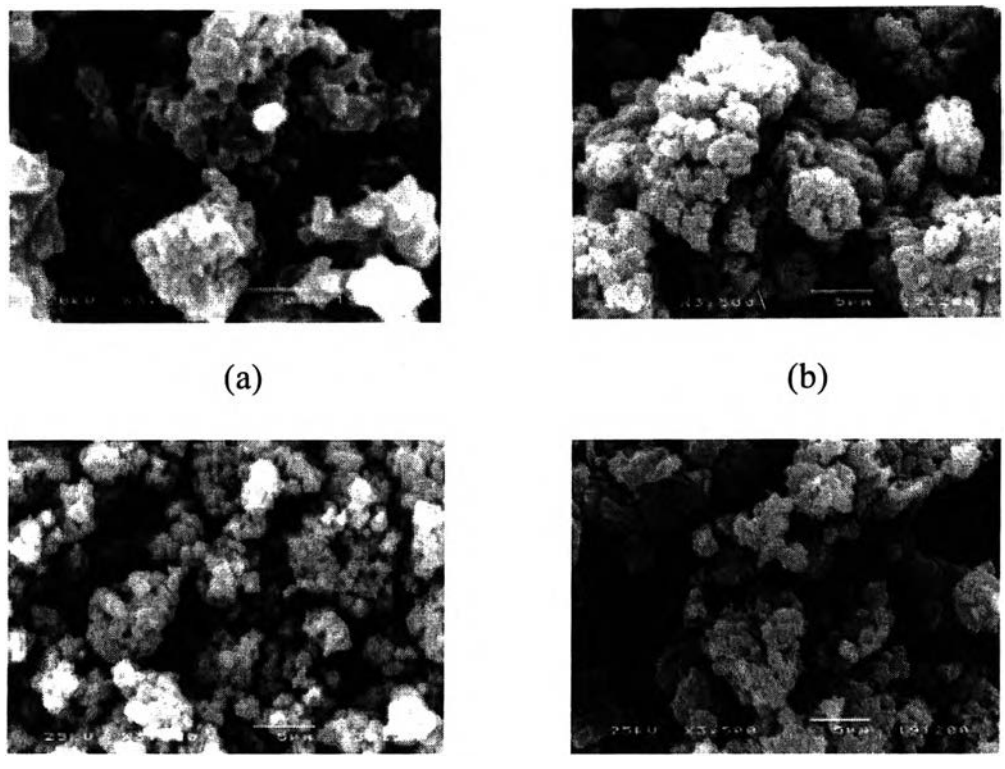

Figure 4.1.5.2 The morphological structure of HBr doped polyaniline at various doping ratios: (a) N_A/N_{EB} = 4; (b) N_A/N_{EB} = 40; (c) N_A/N_{EB} = 200; and (d) N_A/N_{EB} = 1295.

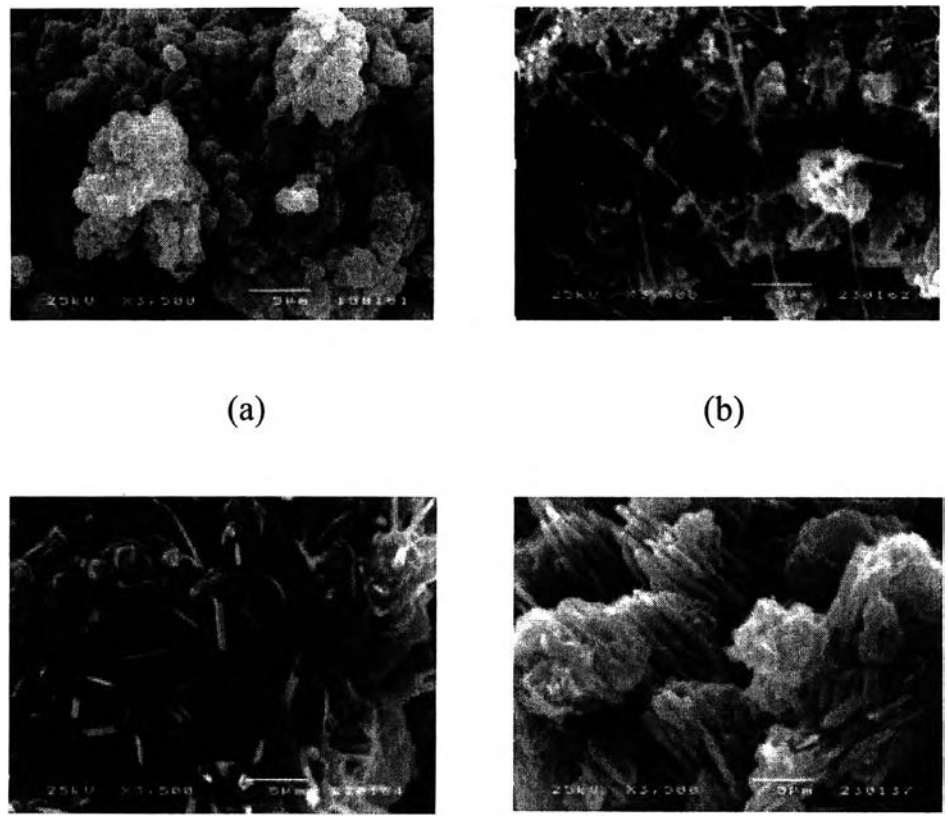

(a) (b)

(c) (d)

Figure 4.1.5.3 The morphological structure of CSA doped polyaniline at various doping ratios: (a) N_A/N_{EB} = 4; (b) N_A/N_{EB} = 40; (c) N_A/N_{EB} = 80; and (d) N_A/N_{EB} = 160.

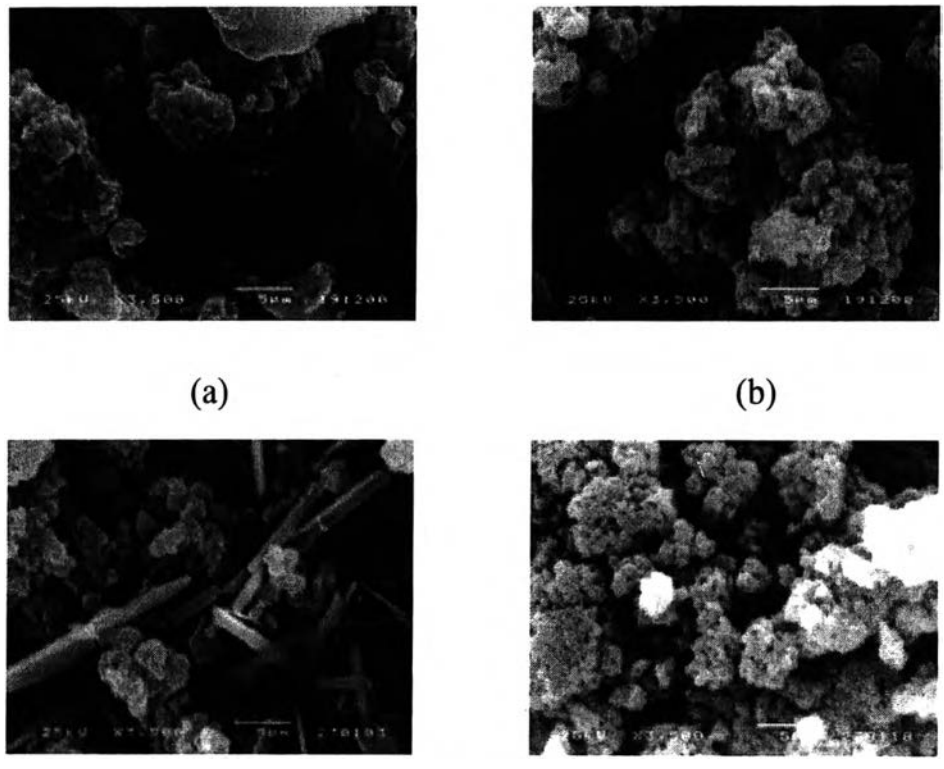

Figure 4.1.5.4 The morphological structure of maleic acid doped polyaniline at various doping ratios: (a) $N_A/N_{EB} = 4$; (b) $N_A/N_{EB} = 80$; (c) $N_A/N_{EB} = 200$; and (d) $N_A/N_{EB} = 500$.

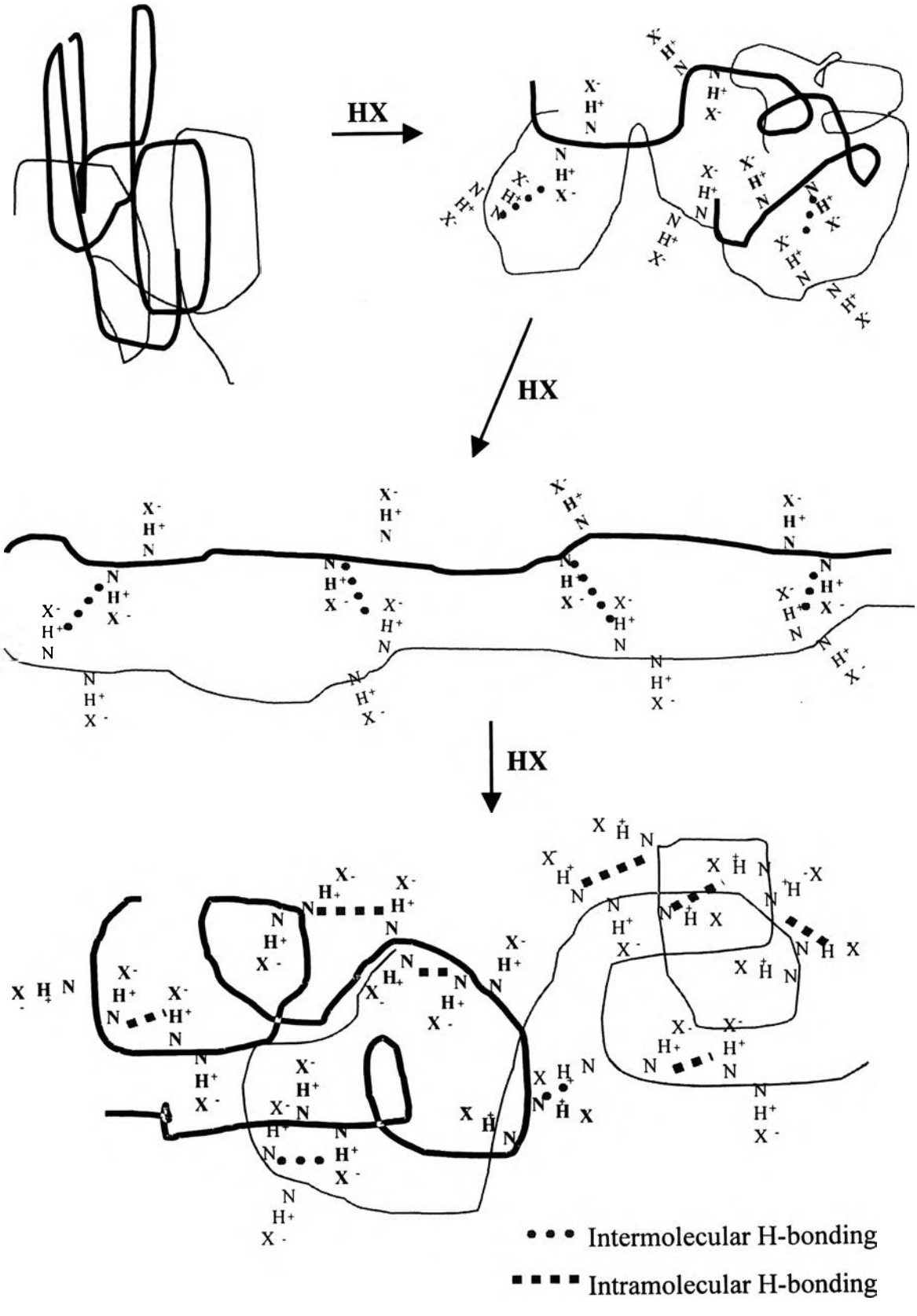

Scheme 4.2 A schematic of morphological structure of maleic acid doped polyaniline.

4.2 Electrical Conductivity of Doped Polyaniline.

4.2.1 Effect of Dopant Types and Doping Ratios on the Specific Conductivity.

By using the four point probe meter, the conductivity of undoped polyaniline, HBr doped polyaniline, camphor sulfonic acid (CSA) doped polyaniline, and maleic acid doped polyaniline was measured at 26-28 °C, relative humidity 68±5°C in the atmospheric pressure.

From Figure 4.2.1.1, in case of HBr doped polyaniline, the conductivity increased dramatically with doping ratio (N_A/N_{EB}) from 4 to 40. This was occurred because some quinoid segments were protonated resulting in an increase in positive charges on the polymer chain and then electrons can delocalize along the chain more effectively. However, the conductivity of higher doping ratios slightly decreased due to the stearic effect of Br^- substituent on the polymer chain resulting to a decrease in the electronic conjugation length. Finally, the conductivity was stable at about 10 S/cm with doping ratio higher than 400 because the conjugation length was stable. The maximum conductivity was about 30 S/cm at doping ratio 40:1.

For CSA doped polyaniline, the conductivity increased significantly at doping ratio 4 because of an increase in the doping level. The conductivity, then, increases gradually until the maximum conductivity was about 10 S/cm at doping ratio 80 due to the occurance of crystallinity and increasing delocalization of electrons in the interchain and intrachain direction. Nevertheless, the conductivity gradually decreased and reached equilibrium at doping ratio 160.

In case of MA doped polyaniline, for doping ratios 2 to 200, the conductivity increased rapidly with doping ratio. The maximum conductivity was about 20 S/cm at doping ratio 200 because the crystallinity was occurred. However, the conductivity of MA doped polyaniline at higher doping ratios

However, the conductivity of MA doped polyaniline at higher doping ratios decreased slowly and trended to stable at doping ratio 500 resulting from the less amount of crystallinity and polaron state.

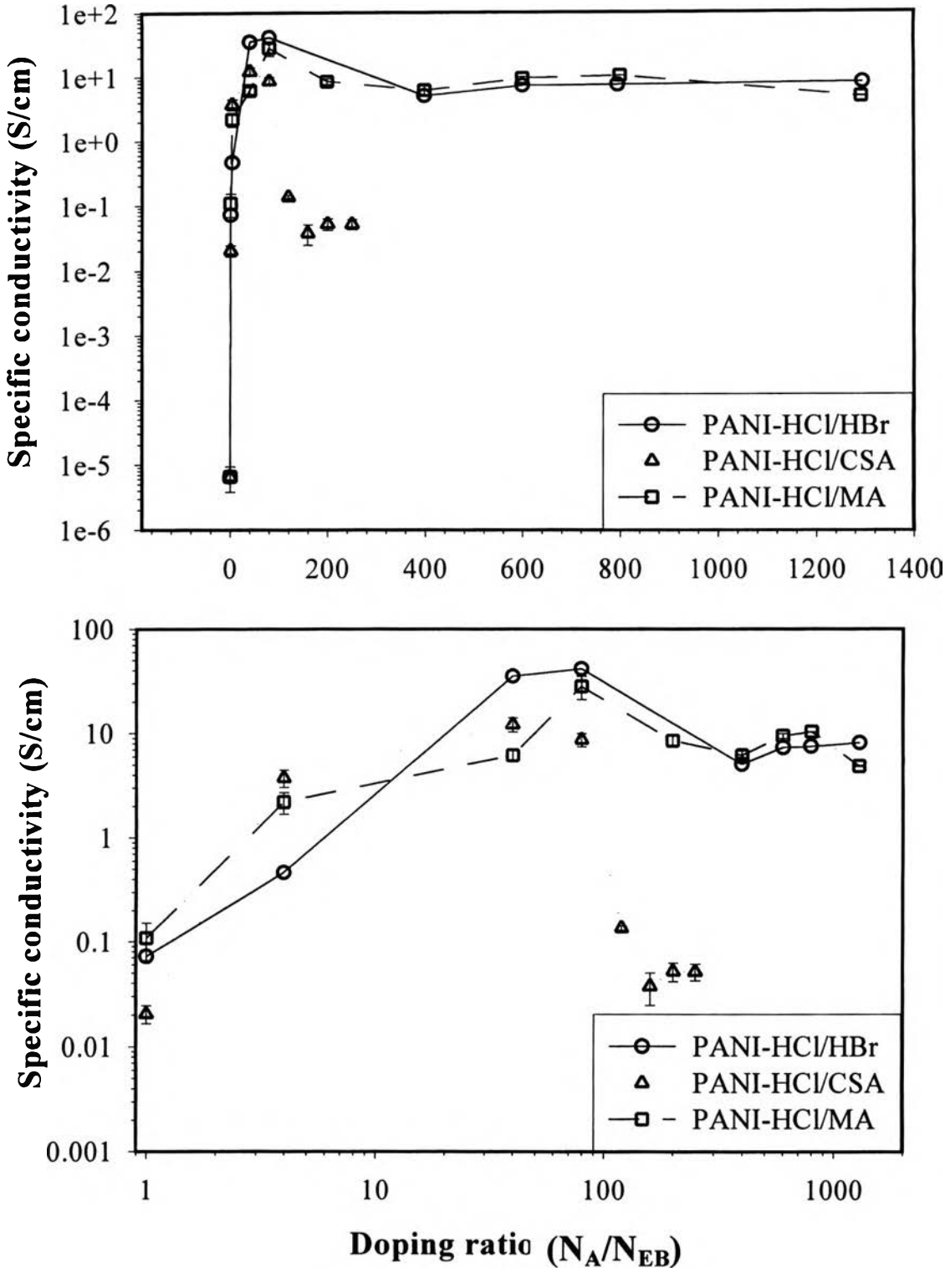

Figure 4.2.1.1 The electrical conductivity as a function of doping ratio (N_A/N_{EB}) of the HBr, CSA, and maleic acid doped polyaniline.

4.2.2 Effect of the Amount of Bipolaron and Polaron on the Specific Conductivity.

From UV-Visible spectrometer, the absorption peaks of the excitation of benzenoid segments, quinoid segments, bipolaron state, and polaron state were identified at about 330, 440, 625, and 805 nm, respectively. The amounts of these electronic structure and the number of charge carrirers were calculated by the method in appendix D and E, respectively. The relationship between the amount of bipolaron and polaron and the specific conductivity is shown in Figure 4.2.2.1.

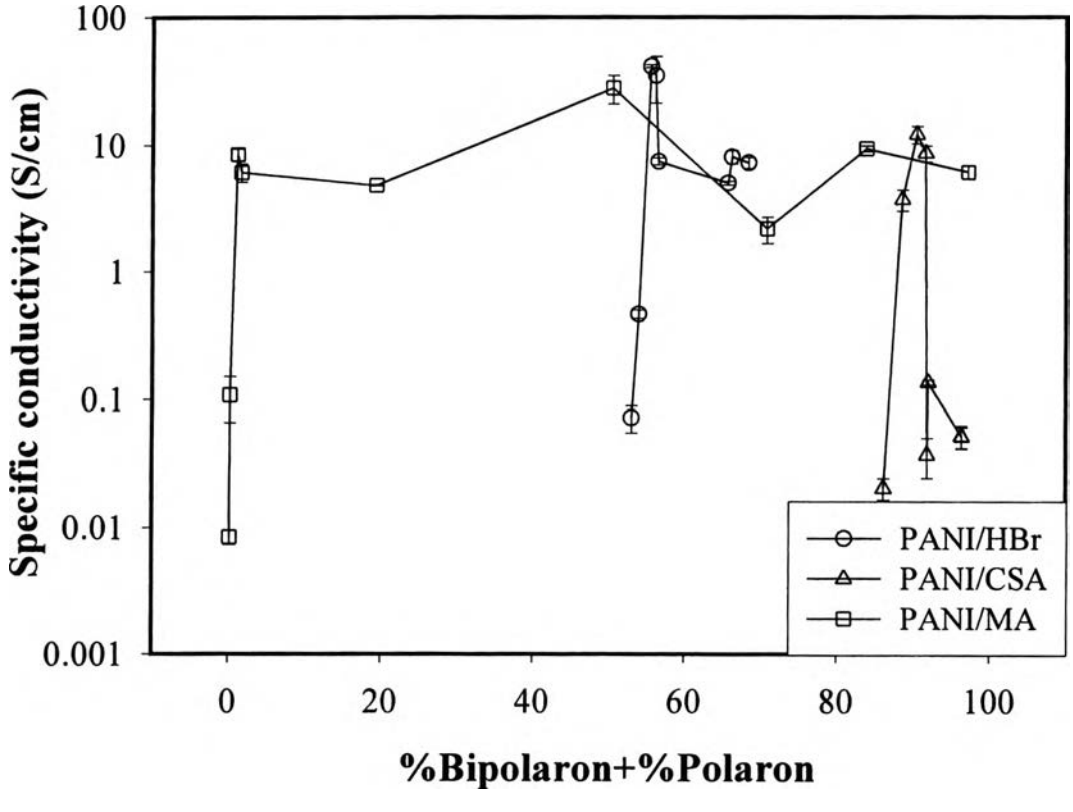

Figure 4.2.2.1 The effect of amount of bipolaron and polaron to the specific conductivity.

From Figure 4.2.2.1, the specific conductivity values of HBr, CSA and maleic acid doped polyanilines increase with the overall percentages of bipolaron and polaron. Nevertheless, the specific conductivity values decrease and become constant at higher percentages of bipolaron and polaron. This suggests that the amount of bipolaron and polaron directly affects the specific conductivity because they are the electron charge carriers which migrate along the chain. However, the graph also indicates that not only the amount of bipolaron and polaron but the other factors such as the morphology can also affect the specific conductivity. The relationship between the conductivity in air and the number of charge carriers is shown in Table 4.7.

Table 4.7 The relationship between the conductivity in air and the number of charge carriers.

Acid	Doping ratio	%BP	%P	%BP+%P	n_{BP}	n_P	N	σ(S/cm)	
								1	2
HBr	1	25.17	27.86	53.03	30.59	16.93	47.52	5.50E-02	8.90E-02
	4	27.84	26.10	53.94	33.84	15.86	49.70	4.28E-01	4.99E-01
	40	25.97	30.12	56.09	31.57	18.30	49.87	2.14E+01	4.93E+01
	80	24.56	30.92	55.48	29.85	18.79	48.64	4.25E+01	4.05E+01
	400	23.54	42.09	65.63	28.62	25.58	54.19	4.87E+00	5.23E+00
	600	22.26	46.09	68.35	27.05	28.01	55.06	8.01E+00	6.64E+00
	800	26.36	30.10	56.47	32.04	18.29	50.33	7.99E+00	6.99E+00
	1295	39.23	26.90	66.13	47.68	16.34	64.03	9.07E+00	7.19E+00
CSA	1	0.918	85.19	86.11	1.12	51.77	52.88	1.65E-02	2.44E-02
	4	0.928	87.59	88.52	1.13	53.23	54.35	3.03E+00	4.46E+00
	40	1.116	89.27	90.39	1.36	54.25	55.61	1.03E+01	1.41E+01
	80	1.534	90.03	91.56	1.86	54.71	56.58	9.94E+00	7.44E+00
	120	1.692	90.26	91.95	2.06	54.85	56.91	1.42E-01	1.30E-01
	160	1.612	90.17	91.78	1.96	54.79	56.75	2.46E-02	5.04E-02
	200	1.380	94.91	96.29	1.68	57.68	59.35	6.26E-02	4.15E-02
	250	0.915	95.38	96.30	1.11	57.96	59.07	6.09E-02	4.22E-02
MA	1	0.137	0.01	0.15	0.17	0.01	0.18	7.31E-03	9.44E-03
	4	0.161	0.02	0.18	0.20	0.01	0.21	1.51E-01	6.59E-02
	40	39.55	10.92	50.47	48.07	6.64	54.71	2.71E+00	1.68E+00
	80	51.28	32.52	83.80	62.33	19.76	82.09	5.47E+00	6.87E+00
	200	18.37	1.01	19.38	22.33	0.61	22.95	2.11E+01	3.52E+01
	400	1.131	0.02	1.15	1.38	0.01	1.39	7.62E+00	9.36E+00
	600	1.262	0.00	1.26	1.53	0.00	1.53	5.13E+00	7.15E+00
	800	25.93	44.91	70.84	31.51	27.29	58.81	8.94E+00	9.93E+00
	1295	3.284	93.85	97.13	3.99	57.03	61.02	1.04E+01	1.03E+01
	1320	1.089	0.01	1.10	1.32	0.01	1.33	4.78E+00	4.93E+00

4.2.3 Effect of CO/N_2 Mixtures on the Electrical Conductivity of Doped Polyaniline.

In this work, the CSA and maleic acid doped polyaniline at various doping ratios were exposed to CO gas at various concentrations in order to investigate the effect of CO/N_2 mixtures on the electrical conductivity. The difference in specific conductivity ($\Delta\sigma$) before and after exposing CO/N_2 mixtures indicated gas sensitivity of doped polyaniline at a particular gas concentration and doping ratio.

The conductivity was measured at 29-32 °C, relative humidity 68± 5°C under pressure 1 atm in $CO-N_2$ environment.

From Figure 4.2.3.1, the change in the electrical conductivity of CSA doped polyaniline when exposed to CO/N_2 mixtures. did not illustrate significantly. It was proposed that the CSA doped polyaniline at doping ratio 20, 80, and 200 did not sensitive to the $CO-N_2$ mixtures.

However the decreasing of the electrical conductivity of maleic acid doped polyaniline at doping ratio 1000 was observed when exposed to the various concentrations of CO/N_2 mixture gas. In contrast, maleic acid doped polyaniline at doping ratios 40, 80, and 200 did not elucidate the difference in the electrical conductivity before and after exposing CO/N_2 mixtures ($\Delta\sigma$). It showed that the decreasing in specific conductivity was independent of doping ratio. Due to CO gas acts as a reducing agent which is electron donor, to the p-type semiconductor polyaniline, the specific conductivity decreased after exposure CO/N_2 mixtures. In case of maleic acid doped polyaniline at doping ratio 1000, the change in the electrical conductivity increased sharply with CO/N_2 mixture gas concentration and then became stable at 500-1000 ppm. For all doping ratios, the sensitivity to CO gas at concentration 0.975 ppm showed the lowest sensitivity because of the less contact area between CO gas and the doped polyaniline chains. Hence, the resultant was the reduction in the sensitivity of doped polyaniline.

Figure 4.2.3.2 showed the minimum CO concentration that the maleic acid doped polyaniline at doping ratios 1000 showed response was less than 2 ppm.

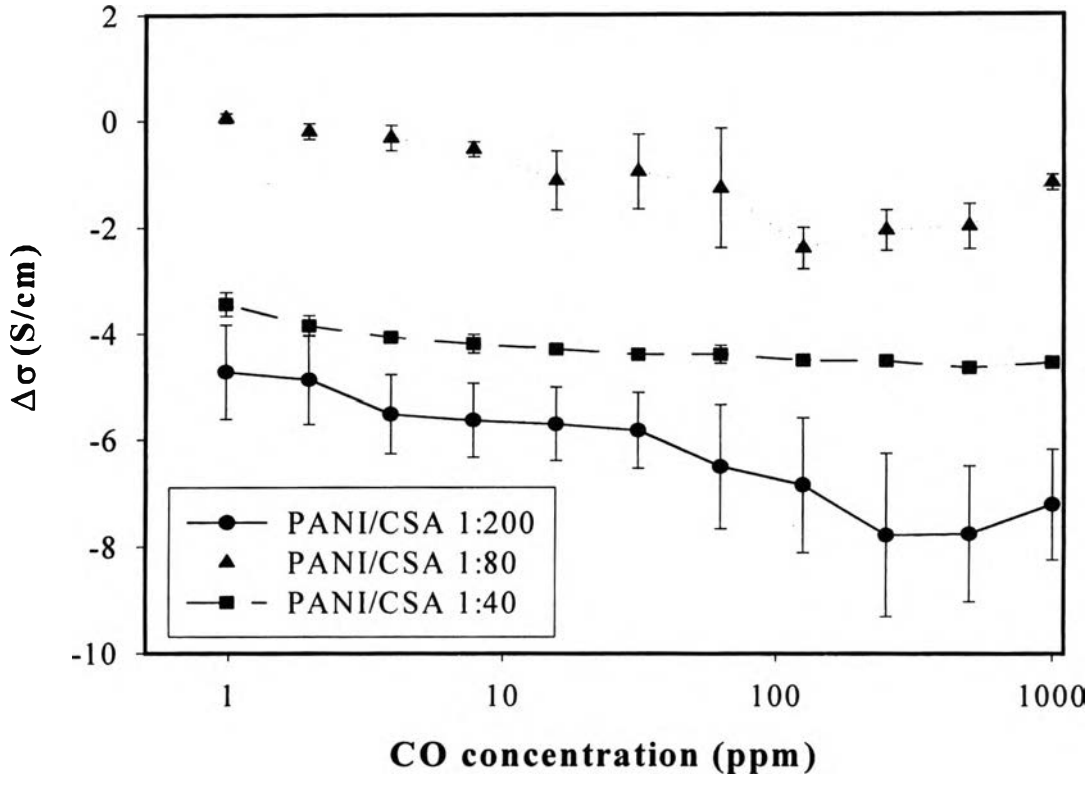

Figure 4.2.3.1 The change in the electrical conductivity as a function of CO gas concentration of the CSA doped polyaniline at various doping ratios.

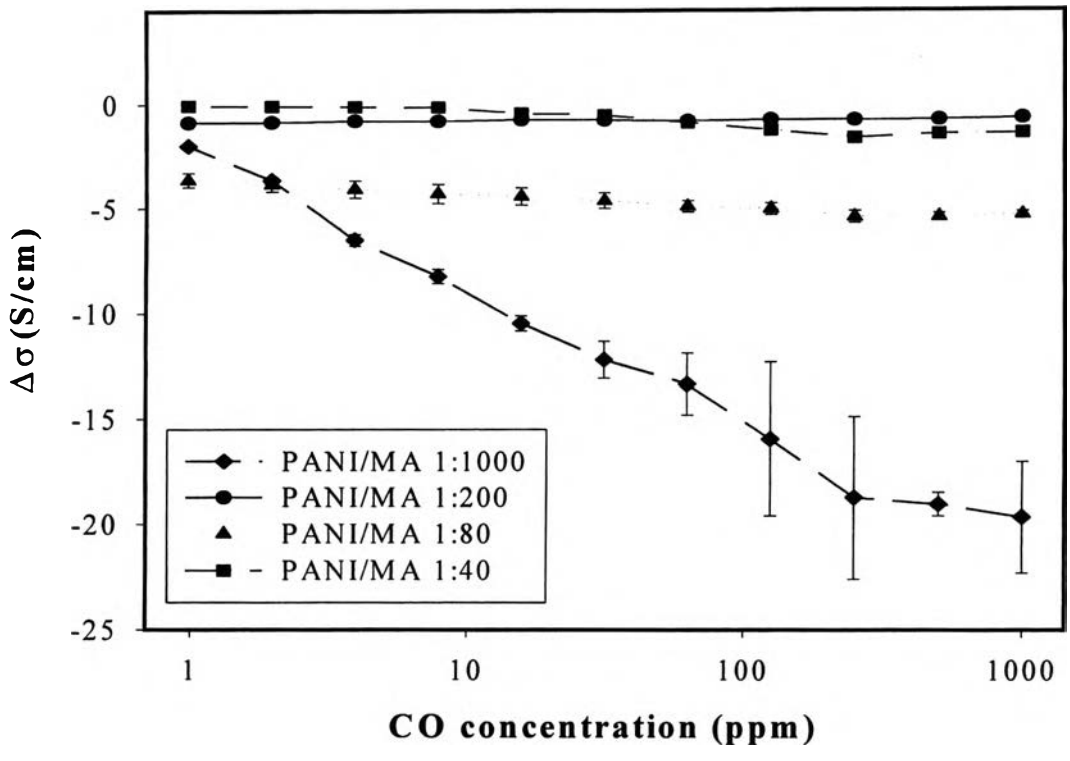

Figure 4.2.3.2 The change in the electrical conductivity as a function of CO gas concentration of the maleic acid doped polyaniline at various doping ratios.

4.2.3 Characterization of Doped Polyaniline after Exposing to a Series of CO/N_2 Mixture Gas by Using FT-IR Technique.

In this work, FT-IR technique was used to investigate the difference in the chemical structure of doped polyaniline after exposing to a CO/N_2 mixture gas. Polyanilines were measured within 24 hours after exposing to a series of CO/N_2 mixture gas. Polyaniline pellets were mixed with KBr and pelletized by using a hydraulic valve press. The sample was pressed under 8 kg/cm^2 for 2 minutes, and then quickly to the FT-IR chamber which is 25-26 °C, relative humidity 55±5°C under pressure 1 atm.

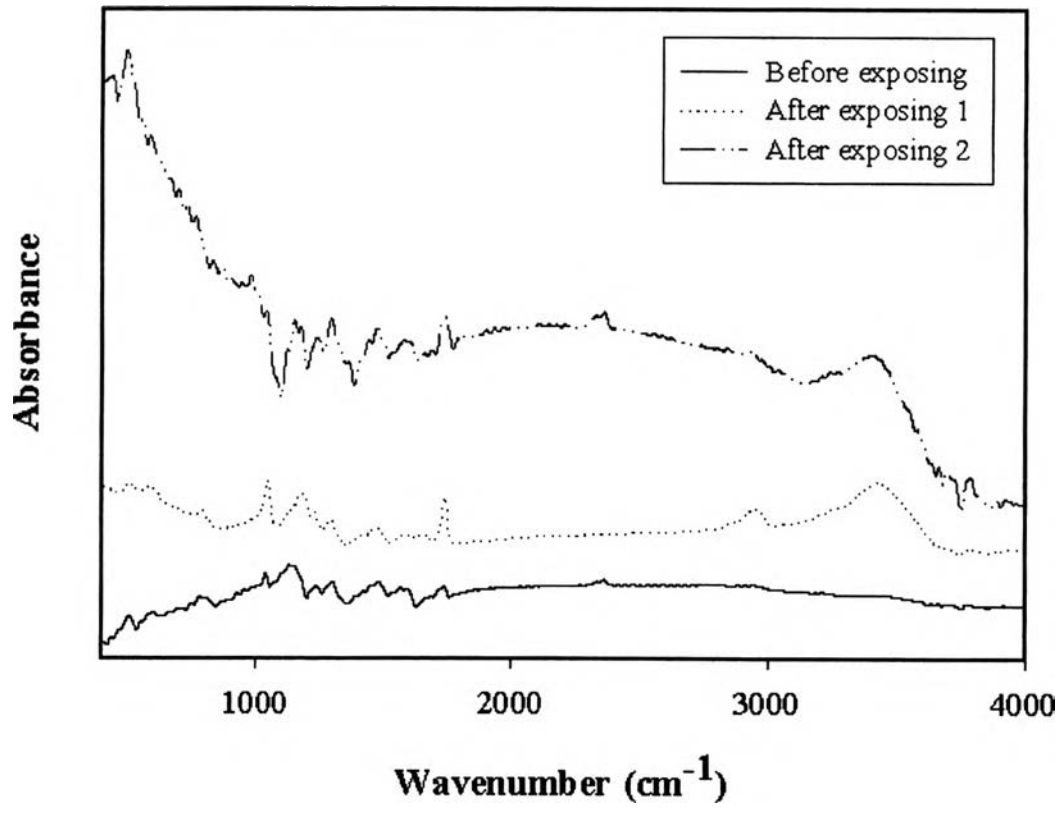

Figure 4.2.4.1 FT-IR spectrum before and after exposing to a series of CO/N_2 mixtures of CSA doped polyaniline at doping ratio (N_A/N_{EB} =200).

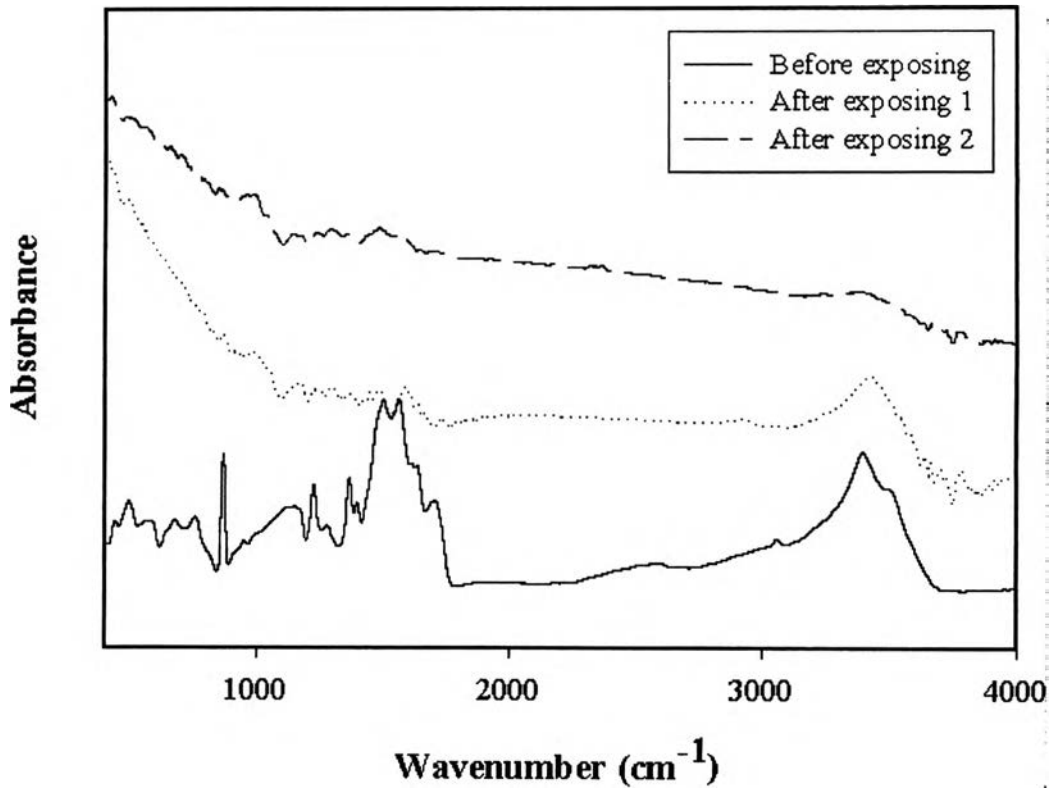

Figure 4.2.4.2 FT-IR spectrum before and after exposing to a seires of CO/N_2 mixtures of maleic acid doped polyaniline at doping ratio (N_A/N_{EB} = 1000).

The assignments of the absorption peaks of FT-IR spectra before and after exposed to CO/N_2 mixtures of doped polyaniline are shown in Table 4.8.

Table 4.8 Assignments of FT-IR absorption bands of before and after exposing to a series of CO/N_2 mixtures of doped polyanilines.

Sample	Before exposing		After exposing	
	Wavenumber (cm^{-1})	Assignment	Wavenumber (cm^{-1})	Assignment
PANI /CSA	3234	N-H stretching	3234	N-H stretching
	1732	Stretching of C=O group of acid	1737	Stretching of C=O group of acid
	1145	A mode of Q=N+H-B or B-NH-B	1051	A mode of Q=N+H-B or B-NH-B
	1035	Sulfonic acid salt group	1038	Sulfonic acid salt group
PANI /MA	3393	N-H stretching	3398	N-H stretching
	1705	Stretching of C=O group of acid	1708	Stretching of C=O group of acid
	1556	C=N stretching of quinoid ring	1559	C=N stretching of quinoid ring
	1496	Streching of benzenoid ring	1499	Streching of benzenoid ring
	1303	C-N stretching of benzenoid ring	1303	C-N stretching of benzenoid ring
	866	C-H out of plane bending of 1,2,4 ring	866	C-H out of plane bending of 1,2,4 ring

The result of the FT-IR measurements is shown in Figure 4.2.4.1-4.2.4.2, namely the FT-IR spectra of CSA and maleic acid doped polyaniline before and after the exposure to a CO/N_2 mixture gas. The graph shows that CO molecules interacted chemically with the doped polyaniline. From FT-IR spectra in Figure 4.2.4.1, it can be seen that the conductivity of polyaniline was destroyed after exposure to CO because the peak at about 3000-4000 cm^{-1} were presented. This suggests that the electron crowd disappeared. In addition, the ratio of peak intensities between 1732, 1145, and 1035 cm-1 changed after doped polyaniline was exposed to the CO/N_2 mixture gas, thus the electrical property of CSA doped polyaniline was altered.

For maleic acid doped polyaniline, polyaniline was destroyed after exposure to the CO/N_2 mixture gas because the ratios of the peak intensities at 1556, 1496, 1303, and 866 cm^{-1}, showing the characteristics of polyaniline, changed. Furthermore, the peak at about 1700 cm^{-1}presenting the stretching of C=O group of maleic acid was rarely observed after an exposure to a series of the CO/N_2 mixture gas.